JOURNAL OF PETROLOGY | VOLUME 37 | NUMBER 2 | PAGES 415–441 | 1996

DER-CHUEN LEE[1], ALEX N. HALLIDAY[1], GARETH R. DAVIES[2], ERIC J. ESSENE[1], J. GODFREY FITTON[3] AND ROBERT TEMDJIM[4]

[1]DEPARTMENT OF GEOLOGICAL SCIENCES, UNIVERSITY OF MICHIGAN, 2534 C. C. LITTLE BUILDING, ANN ARBOR, MI 48109-1063, USA
[2]FACULTEIT DER AARDWETENSCHAPPEN, VRIJE UNIVERSITEIT, 1081 HV AMSTERDAM, NETHERLANDS
[3]DEPARTMENT OF GEOLOGY AND GEOPHYSICS, UNIVERSITY OF EDINBURGH, EDINBURGH EH9 3JW, UK
[4]DEPARTMENT OF EARTH SCIENCES, UNIVERSITY OF YAOUNDE, YAOUNDE, CAMEROON

Melt Enrichment of Shallow Depleted Mantle: a Detailed Petrological, Trace Element and Isotopic Study of Mantle-Derived Xenoliths and Megacrysts from the Cameroon Line

Major element, trace element and Sr–Nd–Pb isotopic compositions of ultramafic xenoliths and megacrysts from the continental Cameroon line provide evidence for metasomatism of the uppermost lithospheric mantle by enriched melts during the Mesozoic. The megacrysts probably crystallized within the lower continental crust from melts similar to the host magmas. All the xenoliths originated as depleted residues after the extraction of basaltic melts, but some indicate evidence of interaction with enriched partial melts before entrainment. The U–Pb isotopic data on garnet are consistent with cooling through >900°C at >300 Ma. The Sm–Nd isotope systematics in constituent phases appear to have been in equilibrium on a xenolith scale at the time of entrainment, indicating derivation from mantle that remained at temperatures >600°C until eruption. Spinel lherzolites that show simple light rare earth element (LREE) depletions are characterized by isotopic compositions that are comparable with, but slightly more depleted than Atlantic N-MORB, suggesting that the unmetasomatized sub-continental lithosphere of the Cameroon line may be isotopically similar to that of sub-oceanic lithosphere. The Nd-depleted mantle model ages of these xenoliths are consistent with late Proterozoic depletion, similar in age to much of the overlying continental crust. In contrast, samples that have LREE-enriched clinopyroxenes (La/Yb = 4·7–9·4) contain trace amounts of amphibole, are enriched in U and have more radiogenic Pb and Sr. These xenoliths yield U–Pb and Sm–Nd model ages consistent with Mesozoic enrichment, in agreement with the age of enrichment of the source regions of the basalts, as deduced from Pb isotopic compositions. Clinopyroxenes record three orders of magnitude enrichment in U and LREE accompanied by progressive K depletion associated with the growth of trace amphibole, with K/U ratios that range from 12 000 to 1. The ratios of the trace elements thought to have similar bulk D in mantle melting, Ce/Pb, Ba/Rb and Nd/Sr ratios, display regional variations related to the time integrated history of enrichments indicated by Nd isotopic compositions. Mass balance calculations suggest that the melts responsible for the most recent enrichment of the lithosphere had higher La/Yb and U/Pb than Cameroon line host magmas, and were probably the product of small degrees of partial melting associated with the earliest stages of the breakup of Pangea.

KEY WORDS: *Cameroon line; mantle xenoliths; megacrysts; REE; isotopic composition; trace element.*

INTRODUCTION

For many years the role of the sub-continental lithosphere in the genesis of intraplate magmas has been hotly debated (e.g. Brooks *et al.*, 1976; Allègre *et al.*, 1981; Allègre, 1982; Fitton & Dunlop, 1985; Dupuy *et al.*, 1988; Halliday *et al.*, 1988, 1990; Hawkesworth *et al.*, 1988; Altherr *et al.*, 1990; Paslick *et al.*, 1995). It is unclear to what extent the isotopic and trace

*Corresponding author.

element compositions of continental basaltic magmas are acquired by reaction with the lithosphere during upward percolation of asthenosphere-derived melts, as opposed to direct melting of the lithosphere (McKenzie, 1985; Navon & Stolper, 1987). Furthermore, sub-continental lithosphere has been proposed by some as a possible source for ocean island basalts, following delamination and asthenospheric entrainment (McKenzie & O'Nions, 1983, 1995). Therefore, determining the composition and development of this poorly characterized reservoir is a critical task.

There are two general approaches to characterizing the isotopic compositions of the lithospheric mantle. The first is to compare basaltic magmas erupted in young oceanic and older continental settings and to ascribe the differences to the effects of the sub-continental lithosphere or crustal contamination (Allègre *et al.*, 1981; Fitton & Dunlop, 1985). The Cameroon line may be the best location on Earth for such an experiment, as it uniquely comprises a genetically related intraplate volcanic chain that extends for 1600 km from ocean islands in the Gulf of Guinea to volcanic centers in the Precambrian cratons of Africa (Fitton & Dunlop, 1985; Halliday *et al.*, 1988, 1990; Lee *et al.*, 1994). However, unless there is a marked difference in trace element and/or isotopic compositions, the role and composition of the lithosphere cannot be readily ascertained (Paslick *et al.*, 1995).

The second and more direct method is to use the ultramafic xenoliths entrained in kimberlites and alkali basalts during ascent and generally considered to be fragments of the sub-continental lithosphere (e.g. Menzies *et al.*, 1987). The isotopic and incompatible trace element compositions of ultramafic xenoliths thought to be derived from the sub-continental lithosphere are known to be extremely heterogeneous. Although the major and trace element chemistry of many ultramafic xenoliths is consistent with their being residues of partial melt extraction (Frey & Prinz, 1978), some ultramafic xenoliths are enriched in incompatible trace elements with or without changes in major element chemistry (Frey & Green, 1974; Dawson, 1982; Galer & O'Nions, 1989). Such trace element enrichment is commonly attributed to interaction with partial melts similar to the host magmas (Kramers *et al.*, 1983; Navon & Stolper, 1987), and/or CO_2–H_2O-rich partial melts that were trapped in the lithospheric mantle (Menzies & Wass, 1983; Andersen *et al.*, 1984; Menzies *et al.*, 1985; O'Reilly & Griffin, 1988; Song & Frey, 1989). Trace element enrichment processes are also considered as probable precursors to the genesis of alkaline magmas (Frey & Roden, 1987; Wilkinson & Le Maitre, 1987). In this paper we present the first isotopic, trace element and major element study of xenoliths from the Cameroon line, and provide evidence of enrichments of the depleted upper mantle that took place at about the same time as those inferred to have occurred in the source regions of the erupted lavas, permitting well-constrained inferences on the relationship between asthenosphere and lithosphere in this region.

The Cameroon line consists of at least 17 plutonic complexes (~65–30 Ma), all in the continental sector, and 12 major volcanic centers (~42 Ma to the present), extending into the Gulf of Guinea (Fig. 1; Fitton & Dunlop, 1985; Fitton, 1987; Déruelle *et al.*, 1991; Lee, 1994; Lee *et al.*, 1994). The only currently active volcano is Mt Cameroon (Fitton *et al.*, 1983), located at the boundary between the oceanic and the continental sectors of the volcanic chain. Basic lavas, ranging in composition from basanite to *hy*-norm basalt, are present in all the volcanic centers except for Etinde, which is composed entirely of nephelinite. The chemical compositions of basaltic lavas are similar between the oceanic and con-

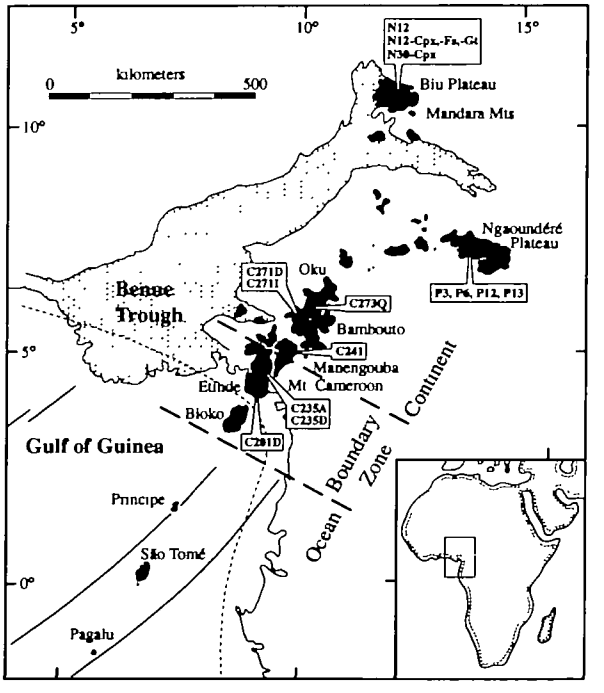

Fig. 1. Geological map showing the major Cenozoic volcanic centers of the Cameroon line and the Gulf of Guinea. The boundary between the continental and oceanic crust (thin broken line) and the oceanic transform faults are taken from Emery & Uchupi (1984) and Sibuet & Mascle (1978), respectively. C201D is from Mt Cameroon; C235A and C235D are from Lake Baronbi Mbo; C241 is from 5 km north of Tombel, C271D and C271I are from Lake Enep; C273Q is from 5 km north-west of Lake Enep; P3, P6, P12 and P13 are from Ngaoundéré Plateau; N12, N12-Cpx, -Gt, -Fs and N30-Cpx are from Biu Plateau.

tinental sectors (Fitton & Dunlop, 1985). Trachyte, trachyphonolite, rhyolite and rare phonolite are the evolved rocks in the continental sector, whereas phonolite and rare trachyte dominate the evolved rocks in the oceanic sector.

The origin of the Cameroon line has been a subject of continuing controversy (Freeth, 1979; Morgan, 1983; Van Houten, 1983; Fitton & Dunlop, 1985; Moreau *et al.*, 1987). Halliday *et al.* (1988, 1990) showed that there is a Pb isotope anomaly at the continent–ocean boundary, and suggested that it resulted from melting of a fossil plume that was emplaced in the Mesozoic. Lee *et al.* (1994) found that in the oceanic sector of the volcanic chain the Sr and Pb isotopic compositions vary systematically in both space and time, and attributed this to an enriched sub-lithospheric 'hot zone' periodically fed and melted by a deep mantle plume.

PETROGRAPHY

Ultramafic xenoliths analyzed in this study were collected around the major continental volcanic centers of the Cameroon line (Fig. 1). Samples C235A and C235D are from near Mt Cameroon at the continent–ocean boundary. Samples C271D, C271I and C273Q are from the vicinity of Bambouto and Oku. Samples P3, P6, P12 and P13 are from the Ngaoundéré Plateau, the eastern extremity of the Cameroon line. Sample N12 is from the Biu Plateau, the northern end of the volcanic chain. In addition, six megacrysts from Mt Cameroon, Manengouba and Biu Plateau have been analyzed. The ultramafic xenoliths are predominantly Group I (Frey & Green, 1974; Frey & Prinz, 1978), or Type I (Menzies, 1983) spinel lherzolites, containing pale green Cr-diopside and brown Cr-spinel. Harzburgite and spinel–garnet websterite are rare. Sample P6 is a spinel–garnet–pargasite websterite that contains Fe–Ti-rich clinopyroxenes, characteristic of Type II xenoliths (Menzies, 1983). The petrography of each sample is as follows.

C235A and C235D. Spinel lherzolites (Lake Baronbi Mbo, near Mt Cameroon)

Both samples are very fresh with sharp grain boundaries, protogranular textures (Mercier & Nicolas, 1975) and no reaction rims. Porphyroblastic olivine and orthopyroxene range from 1 to 5 mm in diameter. Strained pale green clinopyroxenes seldom exceed 2 mm in size. Brown spinels are usually <1 mm, though some range up to 4 mm. Clinopyroxene commonly contains exsolution lamellae of orthopyroxene. Fluid inclusions are found in all mineral phases except spinel, and often form planes, sometimes parallel to grain boundaries, but show no correlation with the orientation of exsolution lamellae. This is consistent with later interactions with fluid-rich (or volatile) reagents. Estimated (visually) modal mineral compositions are 60% olivine, 25% orthopyroxene, 10% clinopyroxene and $\leqslant 5\%$ spinel.

C271D. Spinel lherzolite (Lake Enep, near Oku)

This protogranular sample has similar texture and sharp grain boundaries to C235A and C235D, although reddish brown hematite or iddingsite is found replacing some of the olivine. The modal assemblage contains 55% olivine, 30% orthopyroxene, 10–12% clinopyroxene and $\leqslant 5\%$ spinel. This sample contains trace amounts ($\leqslant 100$ μm) of pargasitic amphibole (Leake, 1978). Fluid inclusions are common and are often associated with grain boundaries.

C271I. Spinel lherzolite (Lake Enep, near Oku)

As with C271D, some of the olivines of this protogranular xenolith are partially replaced by reddish brown hematite or iddingsite. However, compared with C271D, this sample has more orthopyroxene (35%), clinopyroxene (15%), less olivine (45%) and no amphibole. Strained clinopyroxene shows evidence of partial fusion at the grain boundaries.

C273Q. Spinel lherzolite (5 km north-west of Lake Enep, near Oku)

This sample has roughly the same modal compositions and texture as C271I with 45% olivine, 35% orthopyroxene, 15% clinopyroxene and 5% spinel. Some of the clinopyroxenes have reaction rims along the grain boundaries. Brown spinel usually retains sharp contacts with other grains, but reaction rims can be found around small ($<0{\cdot}5$ mm) and irregular spinels. These may be, however, late secondary products. Olivine shows evidence of secondary alteration to reddish brown hematite or iddingsite.

N12. Harzburgite (Biu Plateau)

This sample is the only harzburgite analyzed. The sample is coarse grained with porphyroblastic olivine and orthopyroxene ranging up to 8 mm. Olivine ($\sim$55–60%) and orthopyroxene (40–45%) account for $>95\%$ of the total modal composition. Clinopyroxene makes up $<5\%$, and is generally smaller in size ($\leqslant 1$ mm), probably formed as an exsolution product. No reaction rims are found.

P3. Spinel lherzolite (Ngaoundéré Plateau)

Porphyroblastic olivine measures up to 5 mm but the majority of olivine and orthopyroxene grains are 1–2 mm in diameter. Clinopyroxene and spinel are much smaller, usually <1 mm, yet some primary spinels measure up to 2 mm. Spinel displays reaction rims where in contact with pyroxene. The modal mineral assemblage is estimated at 60% olivine, 25% orthopyroxene, 8% clinopyroxene and 7% spinel. Trace amounts of pargasite amphiboles, $\leqslant 50$ μm, are found in this sample. Some olivines show signs of alteration.

P6. Spinel–garnet–pargasite websterite (Ngaoundéré Plateau)

This is the only sample in which amphibole appears as a major mineral phase, and is also the only Type II xenolith found in this study. Pale gray clinopyroxene, in contrast to the green Cr-clinopyroxene of Type I xenoliths, accounts for 65–70% of the total modal composition (up to 4 mm in diameter). Brown pargasite amphiboles ($\leqslant 20\%$) appear both as a discrete phase and intergrown with clinopyroxene. Pale gray–green orthopyroxene is rare ($\leqslant 5\%$). Gray spinel ($\leqslant 5\%$) is surrounded by pink garnet (5%); both range from 0·5 to 2 mm in diameter. Some garnet is in direct contact with clinopyroxene and amphibole. The texture of this sample is transitional between protogranular and equigranular.

P12. Spinel–garnet websterite (Ngaoundéré Plateau)

This sample has coarse-grained elongate clinopyroxene up to 12 mm in size, fine-grained interstitial orthopyroxene, and scattered spinel ($\leqslant 2$ mm in size) surrounded by fine garnet. There are minor amounts of olivine present. Several veins of secondary carbonate cut across clinopyroxenes. Large clinopyroxenes show exsolved blebs of pale pinkish garnet and orthopyroxene. Garnet also forms as coronas around green spinel with thin pale brown reaction rims at the contacts, and as strings along the pyroxene–pyroxene grain boundaries. Similar textures have been found in xenoliths from eastern Australia (Irving, 1974; Pearson *et al.*, 1991) and Salt Lake Crater, Hawaii (Green, 1966; Beeson & Jackson, 1970). Irving (1974) suggested that these textures reflect exsolution of garnet and orthopyroxene from clinopyroxene, and reaction of clinopyroxene and spinel to yield garnet. None of the mineral phases are optically or chemically zoned. The estimated modal composition is 65% clinopyroxene, 15% orthopyroxene, 10% garnet and 10% spinel.

P13. Spinel lherzolite (Ngaoundéré Plateau)

This sample contains 65% olivine, 25% orthopyroxene, 10% clinopyroxene and 5% spinel. Olivine and orthopyroxene range between 1 and 2 mm in size, whereas clinopyroxene and spinel are usually <1 mm in diameter. The sample is reasonably fresh, and no reaction rims are present, with the exception of some secondary alteration replacing olivine. The texture of this sample is transitional between protogranular and equigranular.

ANALYTICAL METHODS

Each mineral was analyzed at the University of Michigan using a Cameca Camebax electron microprobe in wavelength-dispersive mode with the ZAF reduction method. The acceleration voltage was 15 kV with a beam current of 10 nA and peak counting times of 30 s for each element. A minimum of three measurements were performed for each grain. The results listed in Table 1 are averages of two to four grains. The site occupancy for all the minerals was calculated according to a fixed number of cations: four for pyroxenes, three for spinels and eight for garnets, except for olivine which was normalized to four oxygens. The Fe_2O_3 contents of pyroxenes, spinels and garnets were estimated to yield stoichiometric values of oxygen.

No bulk xenolith chemical analysis was performed owing to variable degrees of alteration of most xenoliths. All mineral separates were purified under a binocular microscope (×50), and each grain was hand-picked to insure that no surface alteration nor mineral or fluid inclusion was present. As most of the xenoliths were friable, the initial disaggregation was done by hand. Mineral separates were then treated in an ultrasonic bath in 2·5 N distilled HCl for 10–15 min to remove surface weathering. Two additional steps of picking under the microscope were subsequently performed. All the mineral separates were picked in either methanol or ethanol, which enhances the optical contrast between the minerals and alteration or inclusions.

All the mineral separates were leached before being dissolved. The leaching procedure was adapted from Zindler & Jagoutz (1988). The minerals were treated twice with 8 ml of hot (~ 90°C) 2·5 N distilled HCl for 20 min, then agitated in an ultrasonic bath for 5 min. The mineral separates were then washed with 8 ml of cold 5% distilled HF for 10 min, and then again agitated in an ultrasonic bath for 5 min. The minerals were then rinsed several times with cold 2·5 N distilled HCl to remove any residual acid left from previous washing steps. All the acids were collected as leachates. The

Table 1a: Representative electron microprobe analyses of olivine

Sample:	C235A	C235D	C271D	C271I	C273Q	N12	P3	P13
SiO_2	40·55	40·66	40·69	40·68	40·43	40·79	40·74	40·66
Al_2O_3	0·03	0·02	0·03	0·08	0·03	0·06	0·01	0·00
Cr_2O_3	—	—	—	0·02	0·01	—	0·02	0·01
FeO	9·91	10·26	8·61	9·73	9·73	8·85	10·02	10·33
MnO	0·16	0·14	0·12	0·16	0·14	0·13	0·15	0·16
NiO	0·38	0·37	0·44	0·35	0·38	0·39	0·37	0·40
MgO	48·74	48·54	49·56	48·88	49·07	49·45	48·74	48·40
CaO	0·11	0·05	0·04	0·16	0·08	0·19	0·05	0·05
Total	99·88	100·04	99·49	100·06	99·87	99·86	100·10	100·01
Si	0·997	0·999	0·998	0·998	0·994	0·998	1·000	1·000
Al	0·001	0·001	0·001	0·002	0·001	0·002	0·000	0·000
Cr	0·000	0·000	0·000	0·000	0·000	0·000	0·000	0·000
Fe	0·204	0·211	0·177	0·199	0·200	0·181	0·206	0·213
Mn	0·003	0·003	0·003	0·003	0·003	0·003	0·003	0·003
Ni	0·007	0·007	0·009	0·007	0·008	0·008	0·007	0·008
Mg	1·787	1·778	1·812	1·787	1·798	1·804	1·783	1·775
Ca	0·003	0·001	0·001	0·004	0·002	0·005	0·001	0·001
Fo	89·8	89·4	91·1	90·0	90·0	90·9	89·7	89·3

mineral separates were rinsed with pure H_2O several times before dissolution.

The minerals were treated sequentially with HF, 30% HNO_3 and 6 N HCl. After the mineral separates were dissolved completely in 6 N HCl, the solution was split, using $\leqslant 15\%$ for isotope dilution, and the remaining solution for isotope composition determination. The aliquots for isotope dilution were spiked with ^{41}K and three other mixed spikes: ^{235}U–^{208}Pb, ^{87}Rb–^{84}Sr and a Ba–REE mixed spike, containing ^{135}Ba and 10 rare earth elements (REE): ^{138}La, ^{142}Ce, ^{150}Nd, ^{149}Sm, ^{153}Eu, ^{157}Gd, ^{164}Dy, ^{168}Er, ^{171}Yb and ^{176}Lu. Chemical separation procedures of U, Pb, Rb and Sr were the same as those of Lee *et al.* (1994). The separation of Ba and REE was achieved using a 3 ml column containing polytetrafluoroethene (PTFE) coated with di(2-ethylhexyl) orthophosphoric acid (H-DEHP), collecting sequentially for Ba, La, Ce, Nd, Sm + Eu + Gd + Dy (collecting in a single aliquot) and Er + Yb + Lu. All the isotopic measurements were made on two VG Sector thermal ionization mass spectrometers equipped with 6 and 7 Faraday collectors, respectively. The analytical procedures for each element and the replication of standards are the same as those of Lee *et al.* (1994).

RESULTS

Mineral chemistry

The Fo content, from 89 to 91% (Table 1a), and the abundances of minor elements (Ni, Mn, Ca) of the olivine are similar to those reported by Simkin & Smith (1970), Frey & Prinz (1978), Stosch (1981) and Galer & O'Nions (1989), typical of Type I ultramafic xenoliths.

Orthopyroxene has generally higher (or equal) *mg*-number [100 Mg/(Mg + ΣFe)] than the Fo content of coexisting olivine in each sample (Table 1b). Compared with the samples that contain Cr-diopsides, the orthopyroxene of P6 has higher TiO_2, Al_2O_3 and ΣFe, and lower Cr_2O_3 and MgO, typical of Type II xenolith (Menzies, 1983). Orthopyroxene from the websterite P12 also has high Al_2O_3 and ΣFe and low Cr_2O_3 and MgO relative to that in spinel lherzolites. However, the very low TiO_2 and the presence of Cr-diopside would favor this sample being classified as a Type I xenolith. The enstatite in the harzburgite has a much higher Wo content (3·7 wt %) than that of all the other xenoliths, possibly indicating a higher equilibration temperature.

In general, clinopyroxene has higher *mg*-number than either the coexisting orthopyroxene or olivine

Table 1b: Representative electron microprobe analyses of orthopyroxene

Sample:	C235A	C235D	C271D	C271I	C273Q	N12	P3	P6	P12	P13
SiO_2	54·76	54·29	55·76	54·28	54·12	55 30	54·95	54·11	54·09	55·65
TiO_2	0·12	0·11	0·04	0·12	0·11	0·06	0·09	0·24	0·05	0·11
Al_2O_3	4·01	3·99	3·45	4·38	4·18	3·02	4·23	4·75	4·77	3·45
Cr_2O_3	0·30	0·26	0·49	0·33	0·33	1·10	0·39	0·06	0·09	0·27
Fe_2O_3	1·08	2·31	0·45	1·81	2·56	0·47	0·31	0·29	1·38	0·11
FeO	5·25	4·61	5·21	4·63	3·94	5·16	6·38	8·90	6·82	6·62
MnO	0·12	0·15	0·12	0·13	0·16	0·14	0·16	0·18	0·14	0·16
MgO	33·09	33·26	33·76	32·91	33 31	32·56	32 69	30·55	31·75	33·06
CaO	0·63	0 47	0·62	0 69	0·63	1·92	0·61	0·73	0·63	0·51
Na_2O	0·09	0·08	0·08	0·15	0·12	0·08	0·04	0·10	0·08	0·06
Total	99·45	99·53	99·98	99·43	99·46	99·81	99 85	99 91	99·80	100·00
Si	1·900	1·885	1·920	1·884	1·878	1 919	1·904	1·894	1·884	1·924
Al^{IV}	0·100	0·115	0·080	0·116	0·122	0·081	0·097	0 106	0·116	0·076
Al^{VI}	0·064	0·048	0·060	0·063	0·049	0 042	0·077	0·090	0·080	0·064
Ti	0·003	0·003	0·001	0·003	0·003	0 001	0·003	0 006	0 001	0 003
Cr	0·009	0·007	0·013	0·009	0 009	0·030	0·011	0·002	0·003	0·007
Fe^{3+}	0·029	0·060	0·012	0·047	0·067	0·012	0·008	0·008	0·036	0·003
Fe^{2+}	0·152	0·134	0·150	0·135	0·114	0·150	0·185	0·260	0·199	0·191
Mn	0·003	0·004	0·003	0·004	0·005	0·004	0·005	0·006	0·004	0·005
Mg	1·711	1·721	1·733	1·703	1·722	1·684	1·688	1·594	1·648	1·704
Ca	0·023	0·017	0·023	0·026	0·023	0·071	0·023	0·027	0·023	0·019
Na	0·006	0·006	0·005	0·010	0·008	0 006	0·003	0 007	0·006	0·004
En	89·3	89·1	90·4	89·1	89·4	87·8	88·7	84·4	86 5	88·9
Fs	9·5	10·0	8·4	9·5	9·4	8·5	10·1	14·2	12·3	10·1
Wo	1·2	0·9	1·2	1·4	1·2	3·7	1·2	1·4	1·2	1·0
mg-no.	90·4	89·9	91·5	90·3	90·5	91·2	89·7	85·6	87·5	89·8

(Table 1c). As with orthopyroxene, the clinopyroxene of P6 has higher Al_2O_3, TiO_2 and Fe, and lower Cr_2O_3 and MgO contents, in contrast to the Cr-diopsides of the spinel lherzolites and the harzburgite (Table 1c). The two sets of microprobe analyses of clinopyroxenes for P12, in contact with spinel and garnet (1) and in contact with orthopyroxene and garnet (2), display negligible difference in composition (Table 1c).

The compositions of spinels are distinctively different between the lherzolites and two websterites. The lherzolites have high $Cr/(Cr+Al+Fe^{3+})$ and low $Al/(Cr+Al+Fe^{3+})$ relative to the websterites (Table 1d), which is consistent with the characteristic differences between Group I and Group II ultramafic xenoliths (Frey & Prinz, 1978). However, spinel from the websterite P12 has *mg*-number indistinguishable from those of the lherzolites.

The chemical compositions of garnets are similar for the two websterites (Table 1e). They both have *mg*-numbers that are higher (~79) than coexisting spinel but lower than clinopyroxene. Garnet in sample P12 has a very similar chemical composition to that of the garnet websterites from Delegate, Australia (Irving, 1974), but has significantly higher MgO and lower ΣFe than those found in the eastern Australia Craton (Pearson *et al.*, 1991).

The compositions of the amphiboles (pargasite) are shown in Table 1f. In general, amphibole in P6 has higher TiO_2 and lower MgO relative to C271D and P3, consistent with the observations in other major mineral phases. The K_2O content is low in amphiboles from both C271D and P3.

Element partitioning between major mineral phases provides a reasonable test of whether the minerals in a xenolith have achieved chemical equi-

Table 1c: Representative electron microprobe analyses for clinopyroxene

Sample:	C235A	C235D	C271D	C271I	C273Q	P3	P6	P12(1)	P12(2)	P13
SiO_2	51·79	52·11	52·59	52·17	52·31	51·85	50·75	52·25	52·44	51·82
TiO_2	0·58	0·63	0·23	0·54	0·56	0·36	1·28	0·29	0·27	0·64
Al_2O_3	6·16	7·17	5·46	6·58	6·42	5·66	7·72	6·46	6·64	6·99
Cr_2O_3	0·62	0·72	1·18	0·73	0·76	0·72	0·09	0·20	0·21	0·75
Fe_2O_3	2·20	1·24	2·48	1·42	1·25	0·56	0·79	0·68	0·04	1·35
FeO	0·82	1·55	0·08	1·79	1·60	2·46	3·21	2 60	3·30	1·49
MnO	0·07	0·05	0·08	0·07	0·05	0·08	0·10	0·06	0·08	0·10
MgO	14·94	13·89	15·08	15·50	14·98	15·31	14·10	14·83	14·80	14·15
CaO	21·24	20·82	21·30	19·86	20·67	21·79	20·11	20·92	20·73	20·71
Na_2O	1·66	2·12	1·89	1·71	1·77	0·99	1·65	1·48	1·43	1·98
Total	100·08	100·30	100·37	100·37	100·37	99·78	99·80	99·77	99·94	99·98
Si	1·872	1·878	1·893	1·876	1 883	1·886	1·846	1·894	1·898	1·874
Al^{iv}	0·128	0·122	0·107	0·124	0·117	0·114	0·154	0·106	0 102	0·126
Al^{vi}	0·136	0·182	0·125	0 154	0·155	0·128	0 177	0·170	0 181	0·172
Ti	0·016	0·017	0·007	0·015	0·015	0·010	0·035	0·008	0·007	0·017
Cr	0·018	0·021	0·034	0·021	0·022	0·021	0·003	0·006	0·006	0·022
Fe^{3+}	0·060	0·034	0·067	0·039	0·034	0·015	0·022	0·018	0·001	0·037
Fe^{2+}	0·025	0·047	0 003	0·054	0·048	0·075	0·098	0·079	0·100	0·045
Mn	0·002	0·002	0·003	0·002	0·002	0·003	0 003	0·002	0·003	0·003
Mg	0·806	0·746	0·810	0·831	0·804	0·830	0·764	0·801	0·798	0·763
Ca	0·823	0·804	0·822	0·765	0·797	0·849	0·783	0·813	0·804	0·803
Na	0·117	0·148	0·132	0·119	0·124	0·070	0·116	0 104	0·100	0·139
En	47·0	45·7	47·6	49·2	47·8	46·9	45·8	46·8	46·9	46·3
Fs	5·0	5·0	4·1	5 5	4·8	5·1	7 2	5·7	5·9	5·0
Wo	48·0	49·3	48·3	45·3	47·4	48·0	47·0	47·5	47·2	48·7
mg-no.	90·5	90·2	92·0	89·9	90·7	90·2	86·4	89·2	88·8	90·3

P12(1), clinopyroxene in contact with garnet and spinel; P12(2), clinopyroxene in contact with garnet and orthopyroxene.

librium (Galer & O'Nions, 1989). This information is critical for the interpretation of thermobarometric calculations and isotopic compositions of clinopyroxene. The variations in Al_2O_3 between pyroxenes and spinels for the Cameroon line xenoliths are shown in Fig. 2a, and indicate that the partitioning of Al follows the relationship of $[Al]^{sp} \gg [Al]^{cpx} > [Al]^{opx}$. The *mg*-number of pyroxenes decreases as the Al_2O_3 of spinel increases. However, there is no clear relationship between Na_2O in pyroxenes and Al_2O_3 in spinel, particularly if the two samples (C271D and P3) that may be affected by the presence of amphibole are ignored (Fig. 2a). The partitioning of Fe–Mg between olivine and pyroxenes (Fig. 2b) follows the relationship of $[mg\text{-number}]^{cpx} > [mg\text{-number}]^{opx} > [Fo]^{ol}$. The partitioning of Cr between pyroxenes and spinel is shown to be $[Cr]^{sp} > [Cr]^{cpx} > [Cr]^{opx}$ (Fig. 2c). From Fig. 2, the partitioning of Al, *mg*-number and Cr among the major mineral phases behave as predicted from crystal field theory (Burns, 1969, 1970), implying that these xenoliths may have reached chemical equilibrium. Galer & O'Nions (1989) suggested that Cr_2O_3 content of pyroxenes saturated at roughly 1·2 wt% for clinopyroxene and 0·6 wt% for orthopyroxene, based on the compositions of ultramafic xenoliths from San Carlos. However, Cr·Al may substitute for Mg·Si in pyroxene. This substitution is buffered for orthopyroxene in spinel lherzolites by Cr-spinel and olivine: $MgCrAlO_4 + MgMgSi_2O_6 = MgCrSiAlO_6 + Mg_2SiO_4$. Similarly, Cr in clinopyroxene is buffered by spinel and olivine via the equilibrium of $MgCr_2O_4 + CaAlSiAlO_6 = MgCrAlO_4 + CaCrSiAlO_6$.

Table 1d: Representative electron microprobe analyses of spinel

Sample:	C235A	C235D	C271D	C271I	C273Q	P3	P6	P12	P13
SiO_2	0·04	0·05	0·03	0·09	0·05	0·03	0·05	0·03	0·02
TiO_2	0·10	0·10	0·07	0·14	0·13	0·06	0·19	0·04	0·05
Al_2O_3	58·17	59·21	49·79	58·10	57·77	53·65	63·51	63·62	58·81
Cr_2O_3	8·57	7·76	18·79	9·47	9·86	12·45	1·18	2·36	8·38
Fe_2O_3	2·41	2·02	1·53	1·71	1·65	3·19	2·33	1·60	1·64
FeO	8·28	9·00	9·39	8·26	8·47	9·85	11·19	10·06	9·37
MnO	0·07	0·08	0·08	0·06	0·07	0·09	0·13	0·09	0·09
MgO	21·34	21·05	19·85	21·51	21·29	19·84	19·91	20·57	20·65
Total	98·98	99·27	99·53	99·34	99·29	99·16	98·49	98·37	99·01
Si	0·001	0·001	0·001	0·002	0·001	0·001	0·001	0·001	0·001
Ti	0·002	0·002	0·001	0·003	0·003	0·001	0·004	0·001	0·001
Al	1·772	1·796	1·568	1·764	1·759	1·672	1·921	1·918	1·794
Cr	0·175	0·158	0·397	0·193	0·201	0·260	0·024	0·048	0·171
Fe^{3+}	0·047	0·039	0·031	0·033	0·032	0·063	0·045	0·031	0·032
Fe^{2+}	0·179	0·194	0·210	0·178	0·183	0·218	0·240	0·215	0·203
Mn	0·002	0·002	0·002	0·001	0·001	0·002	0·003	0·002	0·002
Mg	0·822	0·808	0·791	0·826	0·820	0·782	0·762	0·784	0·797
Y_{Al}	88·9	90·1	78·6	88·6	88·3	83·8	96·5	96·0	89·8
Y_{Cr}	8·8	7·9	19·9	9·7	10·1	13·0	1·2	2·4	8·6
Y_{Fe}	2·3	1·9	1·5	1·7	1·6	3·2	2·3	1·6	1·6
mg-no.	82·1	80·6	79·0	82·3	81·8	78·2	76·0	78·5	79·7

Therefore, the concept of Cr 'saturation' in clinopyroxenes is inappropriate. It is controlled by an exchange reaction of Cr/Al with spinel, which is a function of temperature, the mole fraction of Cr/Al in spinel and, to a lesser extent, pressure.

The variations in major element compositions in these xenoliths can be most simply explained with a partial melting model (Frey & Prinz, 1978). The extraction of basaltic melt preferentially decreases Al_2O_3 and Na_2O contents while increasing the *mg*-number and Cr_2O_3 (Fig. 2) in the residues. Such a melt extraction process might, in principle, be linked to the growth of the local continental lithosphere, or later events such as the formation of the Cameroon line magmas.

Equilibration temperatures and pressures

The equilibration temperatures and pressures for the Cameroon line xenoliths have been estimated (Table 2) using various thermobarometers to avoid probable systematic errors through using a single thermometer or barometer. The thermometers chosen in this study include Fe–Mg partitioning between pyroxenes (Wells, 1977; Brey & Köhler, 1990) and between garnet and clinopyroxene (Ellis & Green, 1979; Krogh, 1988), and Ca, Al, Cr and Na partitioning in phases of pyroxenes and spinel (Hervig & Smith, 1980; Brey & Köhler, 1990; Witt-Eickschen & Seck, 1991). The absence of pressure-sensitive assemblages in spinel lherzolite renders pressure estimates suspect relative to those of garnet lherzolite. A thermobarometer involving partitioning of Ca between olivine and clinopyroxene is available for spinel lherzolite (Köhler & Brey, 1990). Unfortunately, the very low CaO content in olivine, comparable with the detection limit of the electron microprobe, limits its application to natural samples. Three sets of calculations are performed for the garnet websterites (Table 2) based on the same but independently calibrated Al-barometer (Harley, 1984; Nickel & Green, 1985; Brey & Köhler, 1990).

For spinel lherzolites, the estimated equilibrium temperatures fall within the range of 800–1000°C (Table 2), similar to spinel lherzolites reported throughout the world (e.g. O'Reilly & Griffin, 1985;

Table 1e: Representative electron microprobe analyses of garnet

Sample:	P6	P12(1)	P12(2)
SiO_2	41·55	41·50	41·65
TiO_2	0·05	0·04	0·06
Al_2O_3	23·82	23·83	23·84
Cr_2O_3	0·15	0·14	0·16
Fe_2O_3	0·79	0·62	0·81
FeO	8·90	9·00	8·90
MnO	0·33	0·32	0·34
MgO	18·99	18·88	19·07
CaO	5·19	5·21	5·17
Total	99·77	99·54	100·00
Si	2·969	2·971	2·969
Al^{iv}	0·031	0·029	0·031
Al^{vi}	1·975	1·983	1·973
Ti	0·002	0·002	0 003
Cr	0·009	0·008	0·009
Fe^{3+}	0·042	0·034	0 043
Fe^{2+}	0·532	0·539	0·530
Mn	0·020	0·020	0 020
Mg	2·022	2 016	2·026
Ca	0·397	0·400	0·395
mg-no.	79·2	78·9	79·3

P12(1), garnet in contact with spinel and clinopyroxene; P12(2), garnet in contact with clinopyroxene and orthopyroxene.

Table 1f: Representative electron microprobe analyses of amphibole

Sample:	C271D	P3	P6
SiO_2	42·73	42·23	41·57
TiO_2	1·24	0·97	4·14
Al_2O_3	15·01	15·04	15·28
Cr_2O_3	1·54	1·09	0·18
Fe_2O_3	3·78	4·79	4·79
FeO	0·00	0·00	1·64
MnO	0·05	0·06	0·08
MgO	17·52	17·50	15·62
CaO	10·55	11·34	10·22
Na_2O	3·86	3·01	3·61
K_2O	0·01	0·64	0·16
F	0·06	0·03	0·07
Cl	0·05	0·06	0·02
H_2O	1·82	1·87	2·06
–F, Cl=O	–0·04	–0·03	–0·04
Total	98·18	98·60	99·40
T sites			
Si	6·07	6·01	5·93
Al^{iv}	1·93	1·99	2·07
M1, 2, 3, sites			
Al^{vi}	0·58	0·54	0 50
Ti	0·13	0·10	0·44
Cr	0·17	0·12	0·02
Fe^{3+}	0·40	0·51	0·51
Fe^{2+}	0·00	0·00	0·20
Mn	0·01	0·01	0·01
Mg	3·71	3·72	3·32
M4 site			
Ca	1·61	1·73	1·56
Na	0·39	0·27	0·44
A site			
Na	0·67	0·56	0·56
K	0·01	0·12	0·03
O	22·00	22·00	22·00
F	0·03	0·01	0·03
Cl	0·01	0·02	0·01
OH	1·72	1·77	1·96

Neumann, 1991; Nasir, 1992; Zipfel & Wörner, 1992; Princivalle *et al.*, 1994). Pressure estimates for most of the spinel lherzolites using the Ca-barometer are either negative or very low, suggesting that this barometer cannot be applied to natural samples utilizing electron microprobe data. Alternatively, these spinel lherzolites may have reequilibrated at shallow crustal levels; this can be tested by comparing the isotopic compositions of the xenoliths and the host lavas (and/or local crustal samples).

The crustal thickness around the Cameroon line is estimated to be ~30 km (Stuart *et al.*, 1985; Dorbath *et al.*, 1986; Poudjom Djomani *et al.*, 1992), corresponding to a pressure of ~8 kbar for an average crustal density of 2·7 (g/cm^3). Therefore, assuming an average continental geotherm, spinel lherzolites of the Cameroon line were probably sampled by the host alkali basalts at the top of the mantle lithosphere.

The two spinel–garnet websterites have similar temperatures regardless of which thermometer is

Table 1g: XRF analyses of selected megacrysts

Sample:	N12 Fs	N12 Cpx	N12 Gt
SiO_2	60·43	50·01	40·57
TiO_2	0·05	0·59	0·41
Al_2O_3	24·30	8·95	22·87
Fe_2O_3	0·26	7·97	13·50
MnO	0·01	0·16	0·34
MgO	0·07	16·18	16·79
CaO	5·82	15·56	5·64
Na_2O	7·35	0·94	—
K_2O	0·95	—	—
P_2O_5	0·03	0·01	0 02
Total	99·27	100·37	100·14
Nb	0·1	1·4	1·6
Zr	17·7	17·1	47·5
Y	0	8·1	69·4
Th	0	1·4	4
Zn	6·5	36·4	31·9
Cu	0	24·3	68
Ni	2·5	395	160
Cr	0	757	193
Ce	23·6	9·8	9·2
La	6	1·2	0
V	0	254	137
Sc	0	39·9	202

Total Fe as Fe_2O_3. The concentrations of Rb, Sr, Sm, Nd, U and Pb are shown in Table 3.

chosen. However, temperatures estimated using the thermometer of Ellis & Green (1979) are consistently higher than those obtained using other thermometers (Green & Adam, 1991; Adam *et al.*, 1992). If, however, one discards the temperatures of Ellis & Green (1979) and Witt-Eickschen & Seck (1991), all the estimates fall within the range of 990 ± 70°C (within the upper temperature range recorded by the lherzolites). The estimated pressures vary from 14 to 16 kbar, which corresponds to a depth of 50–60 km. This range of pressure and temperature is similar to those reported using older thermobarometers for spinel–garnet pyroxenites from Delegate, Australia (Irving, 1974), and Salt Lake Crater, Hawaii (Green, 1966). However, the estimated temperature and pressure for the spinel–garnet–pargasite websterite, P6, are higher than those experimentally calibrated using natural spinel–garnet–amphibole websterite from Gnotuk Maars, Australia (Adam *et al.*, 1992). The estimated error in pressure assuming a ± 70°C uncertainty in temperature results in 1–2 kbar of uncertainty depending on the barometer chosen. It seems clear that these ultramafic xenoliths last equilibrated in the shallow sub-continental lithospheric mantle.

Leaching experiments

Acid leaching of ultramafic xenoliths before dissolution is designed to remove weathered or superficially metasomatized grain surfaces, so that the residues may be better representatives of the lithospheric mantle. Different leaching procedures have been described (Zindler *et al.*, 1983; Machado *et al.*, 1986; Reisberg & Zindler, 1987; Hamelin & Allègre, 1988); the leaching procedure used in this study was adapted from Zindler & Jagoutz (1988). The percentage of various elements removed by leaching is shown in Fig. 3. As expected, alkalis (Rb and K) are the most mobile elements, and up to 70% is partitioned into the leachate. In contrast, U, Sr and REE are immobile: $<5\%$ of each element was leached. Roughly 3–20% of the total Ba and Pb went into the leachates. The amount of Pb in the leachates may have been slightly overestimated in some instance because of the very low concentration, for which the blank becomes significant. The leaching process does not appear to fractionate the relative concentrations of REE and U. It has been suggested that alkali elements probably reside on grain boundaries in glass or altered phases of mantle xenoliths (Kuo & Essene, 1986; Schiano & Clocchiatti, 1994), consistent with the large quantity of alkalis in the leachates.

Rare earth element compositions

The REE concentrations of various mineral separates determined by isotope dilution are presented in Table 3. In the absence of amphibole or phlogopite, and with the possible exception of high field strength elements (HFSE), clinopyroxene usually contains the dominant inventory of incompatible trace elements in spinel lherzolites. As a result, its REE contents can be used as a good approximation to the bulk xenolith compositions. The chondrite-normalized REE patterns in clinopyroxenes vary from light REE (LREE) depleted to LREE enriched (Fig. 4). Four samples show depletion of LREE with little fractionation of heavy REE (HREE) (Fig. 4a), consistent with small degrees of melt extraction at depths shallower than that corresponding to where garnet is stable. Similar overall REE concentrations and LREE depletion have been documented in other spinel lherzolites (Stosch *et al.*, 1986; Zindler & Jagoutz, 1988; Roden *et al.*, 1988; Roden & Shimizu,

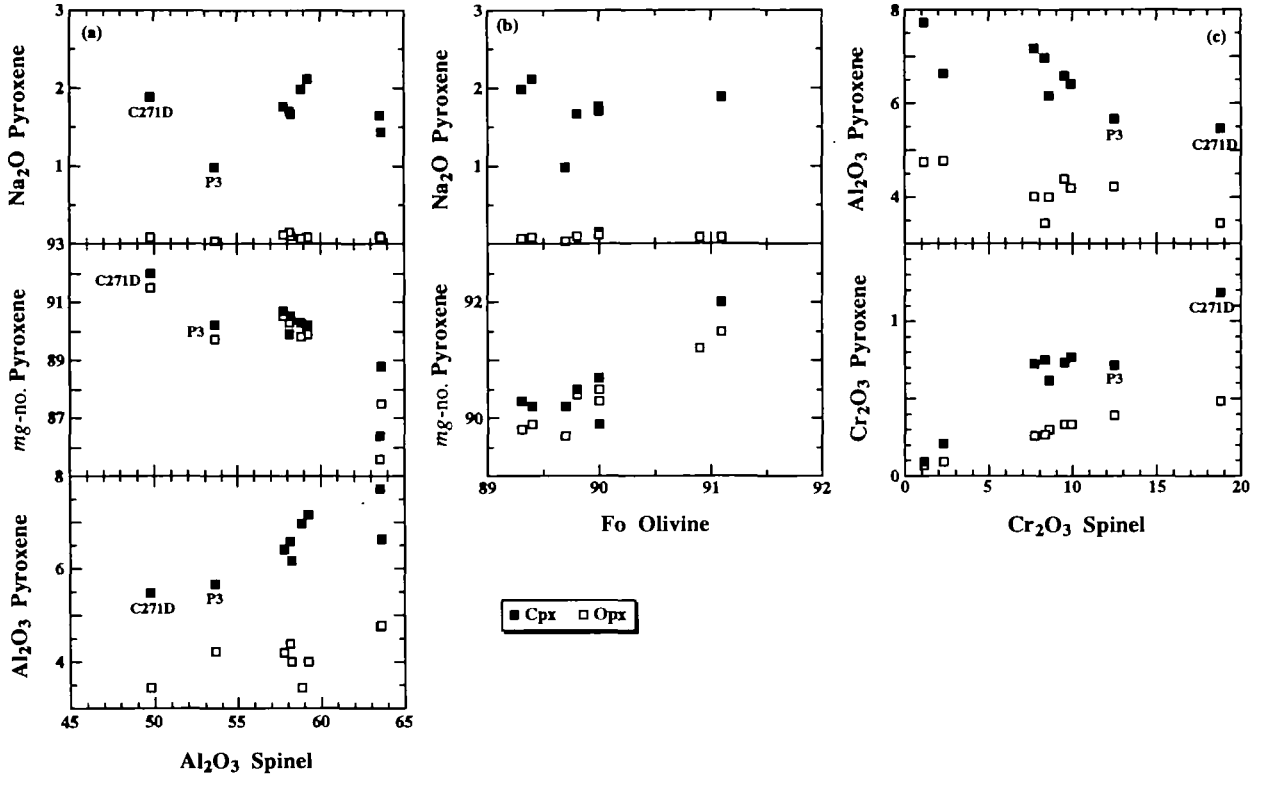

Fig. 2. Plots of Al_2O_3 in spinels vs Al_2O_3, *mg*-number [= Mg/(Mg+total Fe)] and Na_2O in pyroxenes (a), Fo contents in olivines vs *mg*-number and Na_2O in pyroxenes (b) and Cr_2O_3 in spinels vs Cr_2O_3 and Al_2O_3 in pyroxenes (c).

1993), as well as some abyssal peridotites (Johnson *et al.*, 1990). This implies that part of the continental lithospheric mantle of the Cameroon line is chemically similar to sub-oceanic mantle.

Clinopyroxenes from two amphibole-bearing spinel lherzolites, C271D and P3, show enrichments of LREE (Fig. 4b), but have similar flat HREE patterns to those for LREE-depleted samples (Fig. 4a). LREE-enriched partial melts or fluids percolating through the lithospheric mantle are capable of generating the observed LREE enrichments in C271D and P3 (Navon & Stolper, 1987). Some differences in mineral chemistry are also observed in C271D and P3, i.e. anomalously low Na_2O in clinopyroxene, and low Al_2O_3 and *mg*-number and high Cr_2O_3 in spinel (Fig. 3).

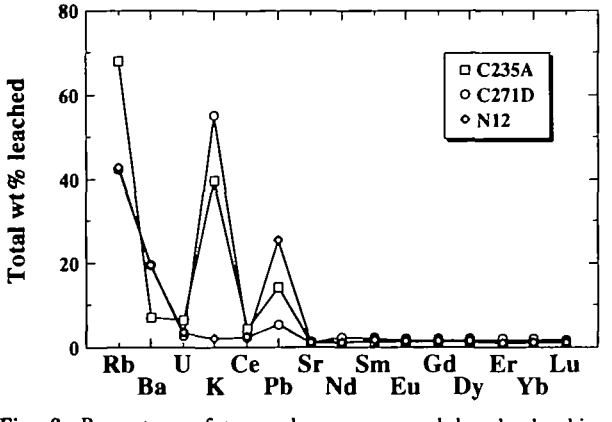

Fig. 3. Percentage of trace element removed by the leaching experiment.

Four samples from the continental interior of the Cameroon line (Fig. 1), N12, P6, P12 and P13, are characterized by depletion in both LREE and HREE (Fig. 4c). Despite their different mineral assemblages, clinopyroxenes from P12 and P13 have identical REE patterns and the lowest overall REE concentrations. Given that P12 is garnetiferous, the similarity of clinopyroxenes in these two xenoliths seems to suggest that the equilibration occurred on a scale larger than that represented by the xenolith. This in turn implies that Nd isotopic compositions of mantle xenoliths cannot be age-corrected beyond the time of eruption with confidence, as the Sm/Nd ratio may not be representative of the same volume as the Nd isotopic composition (see Lee *et al.*, 1993). This is a problem for small coarse-grained garnetiferous xenoliths and could explain why Sm/Nd ratio and Nd isotopic compositions are not correlated in many such samples (Snyder *et al.*, 1993). As a consequence, Sm–Nd model ages are not considered for clinopyr-

Table 2: Estimated temperatures (°C) and pressures (kbar)

Sample:	C235A	C235D	C271D	C271I	C273Q	N12	P3	P6	P12	P13
T(W)	870	820	830	1000	920	—	920	940	940	840
T(BK) 2 px	840	800	780	1040	940	—	910	960	970	830
T(BK) Ca-opx	920	860	920	950	920	1210	920	950	920	880
T(BK) Na-px	970	910	890	1100	1030	—	930	1010	1010	830
T(HS)	960	910	900	1060	1000	—	920	990	990	850
T(WS) Cr–Al-opx	900	840	950	900	870	—	960	850	850	870
T(WS) opx–sp	850	850	710	890	870	—	880	—	—	800
T(EG)	—	—	—	—	—	—	—	1110	1100	—
T(K)	—	—	—	—	—	—	—	1060	1050	—
P(BK) Ca-ol	<0	0·8	<0	<0	<0	—	16	—	—	5
P(H)	—	—	—	—	—	—	—	16·5	15·7	—
P(NG)	—	—	—	—	—	—	—	14·9	14·9	—
P(BK) gt–opx	—	—	—	—	—	—	—	13·8	16·5	—

The thermometers and barometers chosen are: *T*(W), Wells (1977); *T*(BK), Brey & Köhler (1990); *T*(HS), Hervig & Smith (1980); *T*(WS), Witt-Eickschen & Seck (1991); *T*(EG), Ellis & Green (1979); *T*(K), Krogh (1988); *P*(KB), Köhler & Brey (1990); *P*(H), Harley (1984); *P*(NG), Nickel & Green (1985).

oxenes with HREE depletion in subsequent discussions.

The depletion of LREE in P6 and N12 is not as significant as in P12 and P13. Figure 4d illustrates the REE patterns of coexisting minerals from P6. As expected, clinopyroxene and amphibole dominate the LREE to medium REE (MREE), whereas garnet contains the bulk of the HREE. The amphibole of P6 has an REE pattern parallel to that of the clinopyroxene, but with slightly higher overall concentrations. The amphibole is clearly in chemical equilibrium with the clinopyroxene, endorsing the view, based on the major element compositions, that the metasomatism in these xenoliths occurred before entrainment and the last equilibration of the mineral phases. Although garnet was not found in P13 and N12, the HREE depletion suggests that both equilibrated in a larger system that contained garnet.

The REE compositions of orthopyroxene from C271I and P12 are shown in Fig. 4e. Both orthopyroxenes demonstrate HREE enrichment, and the difference between clinopyroxene and orthopyroxene REE contents is more than two orders of magnitude. No REE analysis has been performed on olivine or spinel, which should contain insignificant amounts of REE (Hanson, 1980; Kramers *et al.*, 1983; McKay, 1989; McKenzie & O'Nions, 1991; Kennedy *et al.*, 1993).

Other incompatible trace elements

The concentrations of U, Pb, Rb, Sr, Ba and K in the mineral separates were also determined by isotope dilution (Table 3). All the plots shown in Fig. 5 are normalized to the trace element compositions of primitive mantle (Sun & McDonough, 1989). The four samples that show LREE-depleted patterns exhibit depletion of the most incompatible elements, e.g. Rb and Ba, and gradual enrichment of less incompatible elements such as Sr, Nd and Sm (Fig. 5a). In all four samples U is much less depleted than K, and the variations in both U and K exceed the variations for other elements despite their very similar incompatibility in the mid-ocean ridge basalt (MORB) source (Jochum *et al.*, 1986). This combined enrichment of U and depletion of K is even more obvious in the two LREE-enriched samples, C271D and P3 (Fig. 5b). In general, Rb, Ba and K are consistently depleted, whereas U can be either depleted or enriched, correlated with the behavior of the LREE. The Pb abundance of C271D also shows clear enrichment, but Pb is depleted in P3. The four samples that show both LREE and HREE depletions are plotted in Fig. 5c. They also show depletions in Rb, Ba and Pb (only in N12 and P6) relative to other elements. However, again these elements are not as variable as K and U. The trace elements Ba,

Table 3: Trace element concentrations

Sample:	Min.	Rb*	Sr	U*	Pb	K	Ba	La	Ce	Nd	Sm	Eu	Gd	Dy	Er	Yb	Lu
Xenoliths																	
C235A	cpx	2·84	69·1	11·4	0·107	3·64	0·168	1·08	4·29	4·088	1·661	0·684	2·67	3·35	2·18	1·92	0·299
C235D	cpx	1·27	59·9	13·3	0·132	2·19	0·0896	0·771	3·03	3·286	1·379	0·579	2·28	2·99	1·93	1·74	0·257
C271D	cpx	3·15	33·37	777	0·408	0·967	0·203	6·96	7·29	2·392	1·144	0·482	1·99	2·59	1·71	1·48	0·23
C271I	cpx	3·39	63·17	3·69	0·144	27·6	0·26	0·594	3·01	3·612	1·574	0·662	2·63	3·41	2·24	1·95	0·288
	opx	1·82	0·249	0·99	—	0·39	—	0·00457	—	0·0300	0·0218	0·0130	0·105	0·145	0·171	0·266	0·0489
C273Q	cpx	2·47	56·1	50·9	0·182	12·7	0·204	0·599	2·51	3·085	1·303	0·644	2·12	2·69	1·73	1·48	0·205
N12	cpx	9·69	140·9	12·8	0·0895	155	0·387	2·06	7·01	5·074	1·390	0·499	1·55	1·06	0·464	0·342	0·0545
	opx	—	—	—	—	—	—	—	—	0·158	0 0699	—	—	—	—	—	—
P3	cpx	12·1	148·1	231	0·254	2·77	0·53	14·8	27·5	8·354	1·517	0·565	1·99	2·488	1·62	1·57	0·244
P6	cpx	7·12	103·9	50·1	0·0993	2·67	0·422	4·67	15·4	13·99	4·002	1·36	4·34	3·3	1·23	0·634	0·0657
	amp	4300	425·1	41·2	0·452	610	71·7	5·65	18·0	16·33	4·717	1·67	5·82	4·02	1·58	0·893	0·108
	gt	6·76	13·9	5·82	0·0264	36·8	0·403	0·0341	0·218	0·7686	1·039	0·672	4·04	10·9	11·4	13·0	1·80
P12	cpx	4·63	36·14	1·43	0·0612	5·37	0·402	0·495	1·72	1·769	0·6998	0·287	1·11	0·995	0·379	0·23	—
	opx	1·45	1·33	—	0·0023	1·38	0·039	0·00174	0·00867	0·0105	0·00775	0·00425	0·0226	0·0437	0·0348	0·0412	0·0063
P13	cpx	2·42	36·72	1·52	0·0680	4·82	0·862	0·481	1·74	1·775	0·7015	0·285	1·14	0·987	0·432	0·34	0·0298
Megacrysts																	
C201D	cpx	5·31	64·16	2·9	0·045	6·65	0·225	1·82	7·10	6·887	1·988	0·659	2·14	1·62	0·706	0·471	0·0729
C241	fs	878	1964	—	—	573	242	8·36	10·4	2·403	0·219	0·728	0·208	0·035	0·050	0·0213	0·020
N12	gt	196	1·67	18·7	0·498	44·6	17	—	0·556	1·280	1·188	0·710	3·87	3·66	8·92	9·905	1·59
N12	fs	2880	3945	—	1·35	8176	528	—	1·12	2·830	0·283	0·961	0·192	0·0398	0·0234	0·0136	0·0019
N12	cpx	12·4	37·63	4·44	0·0369	26·0	0·32	0·936	3·34	3·546	1·234	0·459	1·67	1·53	0·798	0·592	0·0564
N30	cpx	4·51	143·2	—	—	35·3	0·386	5·44	21·9	25·39	8·526	2·95	8·98	4·56	0·778	0·211	0·0130

Cpx, clinopyroxene; opx, orthopyroxene; amp, amphibole; gt, garnet; fs, feldspar. The concentrations shown are in p.p.m., except for those with *, which are in p.p.b. All measurements performed by isotope dilution.

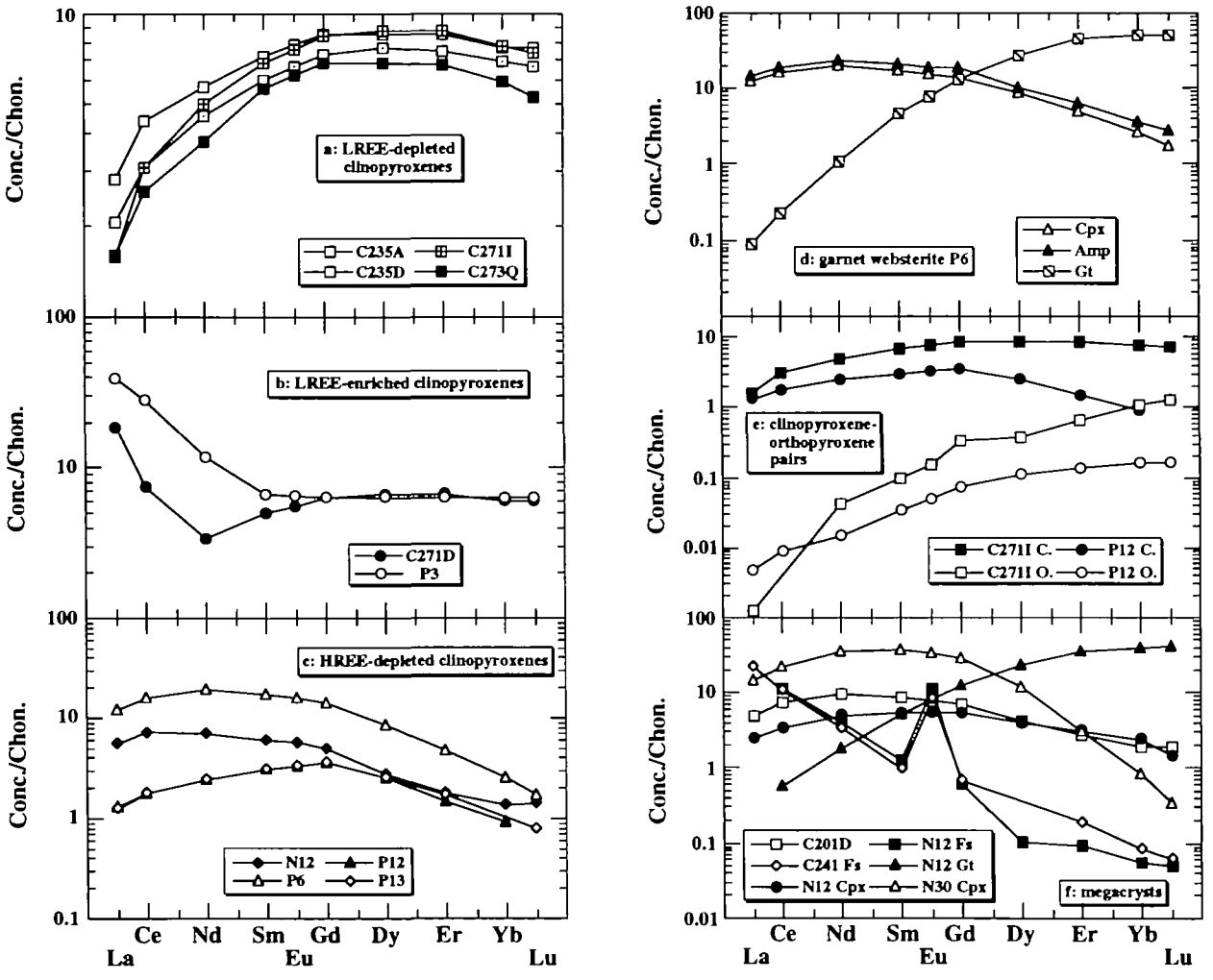

Fig. 4. Chondrite normalized rare earth element compositions of clinopyroxene (a, b and c), coexisting amphibole and garnet (d), orthopyroxene (e), and megacrysts (f). The normalizing values are taken from Masuda *et al.* (1973).

Rb and Pb are relatively uniform, varying by less than one order of magnitude, in contrast to U and K, which vary by over two orders of magnitude. Again, the most U-rich sample (P6) is the most K depleted. The harzburgite, N12, has the highest K and moderate U contents, distinct from the patterns of clinopyroxene from spinel lherzolites, in which the clinopyroxenes are enriched in U but depleted in K (Fig. 5a and b).

The clinopyroxene in the websterite P6 shows the same extreme K/U fractionation found in P3 and C271D (Fig. 5c), and all three samples contain amphibole, which provides clear evidence that LREE and U enrichment is coupled with the growth of amphibole, resulting in the depletion of K in the coexisting clinopyroxene (Fig. 5d). The amphibole is enriched in Rb, Ba, K, Pb and Sr relative to coexisting clinopyroxene. However, the U and REE contents of clinopyroxene and amphibole are very similar. Trace amounts of amphibole are found in both C271D and P3, but these were difficult to separate for analysis owing to the small grain size. If the partitioning of K and U between amphibole and clinopyroxene in P6 (Table 4) is applied to C271D and P3, the approximate bulk rock trace element compositions for these two samples can be calculated (Table 5). This estimate does not consider contributions from olivine or spinel, owing to their very low incompatible trace element concentrations. Compared with the unmetasomatized samples (C235D and C271I), C271D and P3 have significantly higher bulk rock Rb, Ba, U, La, Ce and Pb concentrations (Table 5). The K depletions in the clinopyroxenes of C271D and P3 are compensated by the presence of trace amounts of amphibole, which yield bulk rock compositions indistinguishable from C271I. The

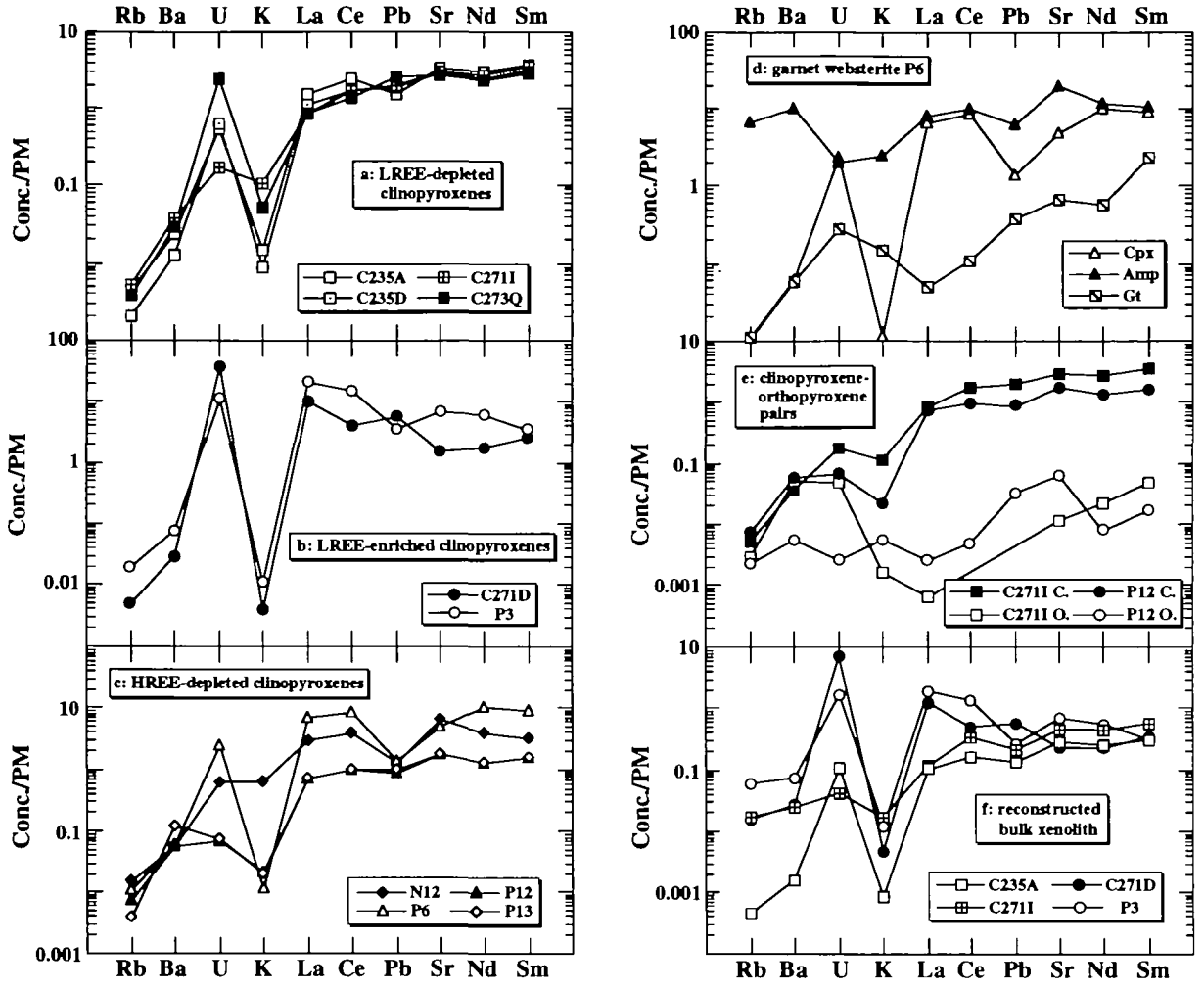

Fig. 5. Primitive mantle normalized trace element compositions of clinopyroxene (a, b and c), coexisting amphibole and garnet (d), orthopyroxene (e), and reconstructed bulk xenolith (C235D, C271D, C271I and P3) composition (f) The normalizing values are taken from Sun & McDonough (1989).

presence of amphibole and the U and LREE enrichment in C271D and P3 are clearly equilibrium features caused by metasomatism some considerable time before entrainment.

Although the K/U ratios in the clinopyroxenes vary through four orders of magnitude from 1 to >10000, the Ba/Rb ratios of all clinopyroxenes are relatively consistent (Fig. 6), with the exception of P13. However, the Ba/Rb ratios are significantly higher than those found in MORB and ocean island basalt (OIB) (Hofmann & White, 1983; Fig. 6). The Ba/Rb ratios of the clinopyroxenes tend to decrease slightly with increasing Rb concentration (Fig. 6), suggesting that varying degrees of depletion have had only a small effect on the Ba/Rb ratios and that Ba is slightly less incompatible than Rb. The K/U ratios of clinopyroxenes, excluding C271D, P3 and P6 that contain amphibole, range from 166 to 12000. This range includes all OIBs, and reaches to N-type MORB (Sun & McDonough, 1989). The K/U is one of the most variable incompatible trace element ratios in OIB, probably reflecting the role of amphibole as a fractionating phase at very small degrees of partial melting (Halliday *et al.*, 1995).

The large K depletion relative to the primitive mantle in the clinopyroxenes of the LREE-depleted spinel lherzolites also records a significant trace element fractionation process. Although clinopyroxenes of P3 and C271D are relatively depleted in K compared with all other clinopyroxenes, calculated whole rocks are not depleted in K, owing to high K contents in amphibole (Table 5). A possible explanation of K depletion in other xenoliths is that they were also hydrated, followed by the preferential removal of amphibole either by a later melting event or upon decompression during emplacement. The

Table 4: Apparent mineral–mineral partition coefficients

Element:	C271I Opx–Cpx	P12 Opx–Cpx	P6 Amp–Cpx	P6 Gt–Cpx
Rb	0·537	0·314	599	0·961
Ba	—	0·0975	170	0·956
U	0·282	—	0·825	0·121
K	0·0162	0·259	220	13·3
Pb	—	0·0403	4·53	0·274
Sr	0·00394	0·0369	4·09	0·134
La	0·000769	0·00351	1·21	0·00732
Ce	—	0·00503	1·16	0·0141
Nd	0·00831	0·00595	1·17	0·0549
Sm	0·0139	0·0111	1·18	0·260
Eu	0·0196	0·0148	1·23	0·494
Gd	0·0399	0·0204	1·34	0·932
Dy	0·0425	0·0439	1·22	3·29
Er	0·0763	0·0918	1·29	9·32
Yb	0·136	0·179	1·41	20·5
Lu	0·170	—	1·64	27·4

Table 5: Reconstructed whole-rock trace element compositions

Element:	C235D	C271I	C271D	P3
Rb	0·0003	0·0011	0·010	0·039
Ba	0·011	0·16	0·20	0·51
U	0·0023	0·0009	0·16	0·036
K	0·23	4·3	1·2	3·3
La	0·077	0·089	0·88	1·3
Ce	0·31	0·61	0·93	2·4
Pb	0·026	0·042	0·11	0·051
Sr	6·05	9·57	4·72	14·9
Nd	0·34	0·55	0·31	0·74
Sm	0·14	0·24	0·15	0·14

The trace element concentrations of olivine and spinel are ignored. The concentrations of orthopyroxene and amphibole are calculated according to the mineral–mineral partition coefficients listed in Table 5. The amounts of amphibole in C271D and P3 are set to be 0·5 wt %. All elements are expressed as p.p.m.

large variations in K contents of clinopyroxene from spinel lherzolites can be explained if there is formation and removal of amphibole as a consequence of enrichment and depletion by small degree partial melts. The D values calculated in Table 4 indicate that K removal via amphibole melt would also deplete the xenolith in Rb relative to Ba and explain the non-MORB-like Ba/Rb. Such a model is supported by the decrease in Ba/Rb with increasing Rb shown in Fig. 6.

Hofmann *et al.* (1986) showed that the Ce/Pb ratio in MORB and OIB is fairly uniform (25 ± 5) and represents the present-day upper-mantle Ce/Pb ratio. The range of Ce/Pb ratios of clinopyroxenes varies from 13·5 to 154, much larger than the suggested range for the upper mantle. However, Halliday *et al.* (1995) showed that Ce/Pb tends to be higher (extending up to 90) in OIB from regions of older oceanic lithosphere. This is paralleled by the Cameroon line xenoliths. That is, the Ce/Pb ratios are higher in the continental interior, where the lithosphere is probably older. Those xenoliths from the continental margin are in closer agreement with average OIB and MORB ($Ce/Pb = 23 \pm 10$). If only LREE-depleted clinopyroxenes are chosen, the range of Ce/Pb is further restricted. OIB display a positive correlation between Ce/Pb and U/Pb (Halliday *et al.*, 1995), and no correlation between Ce/Pb and Ce/U. The xenolith clinopyroxenes, however, display no clear relationship between Ce/Pb and U/Pb, nor between Ce/U and Ce/Pb (Fig. 6).

Ratios of other trace elements that should have similar mineral–melt bulk D values also display a very simple relationship with geography. That is, clinopyroxene from the continental margin xenoliths, where the lithosphere is probably younger, have lower and more uniform Ba/Rb and Sr/Nd ratios than clinopyroxene from the interior. The Ba/Rb ratios are particularly significant because they are very uniform in the five samples from the continental margin (71 ± 9), despite the large degrees of variability in degrees of trace element enrichment superimposed on depletion (U = 3·7–777 p.p.b.), and the greater leachability of Rb relative to Ba (Fig. 3).

Mineral–mineral partition coefficients

Mineral–mineral partition coefficients for various incompatible trace elements for coexisting minerals that are in 'chemical equilibrium' were calculated from our concentration data (Table 4). The range of orthopyroxene–clinopyroxene partition coefficients from this study fall within the range of those reported by Stosch (1982) and Zindler & Jagoutz (1988), significantly lower than the older values reported by Philpotts *et al.* (1972), Stueber & Ikramuddin (1974), Dasch & Green (1975), Hanson (1977), Basu & Murthy (1977), Ottonello *et al.* (1978) and Ottonello (1980). Zindler & Jagoutz (1988) attributed the differences to inclusions or impurities in the mineral separates of earlier workers owing to the poorer lighting employed then com-

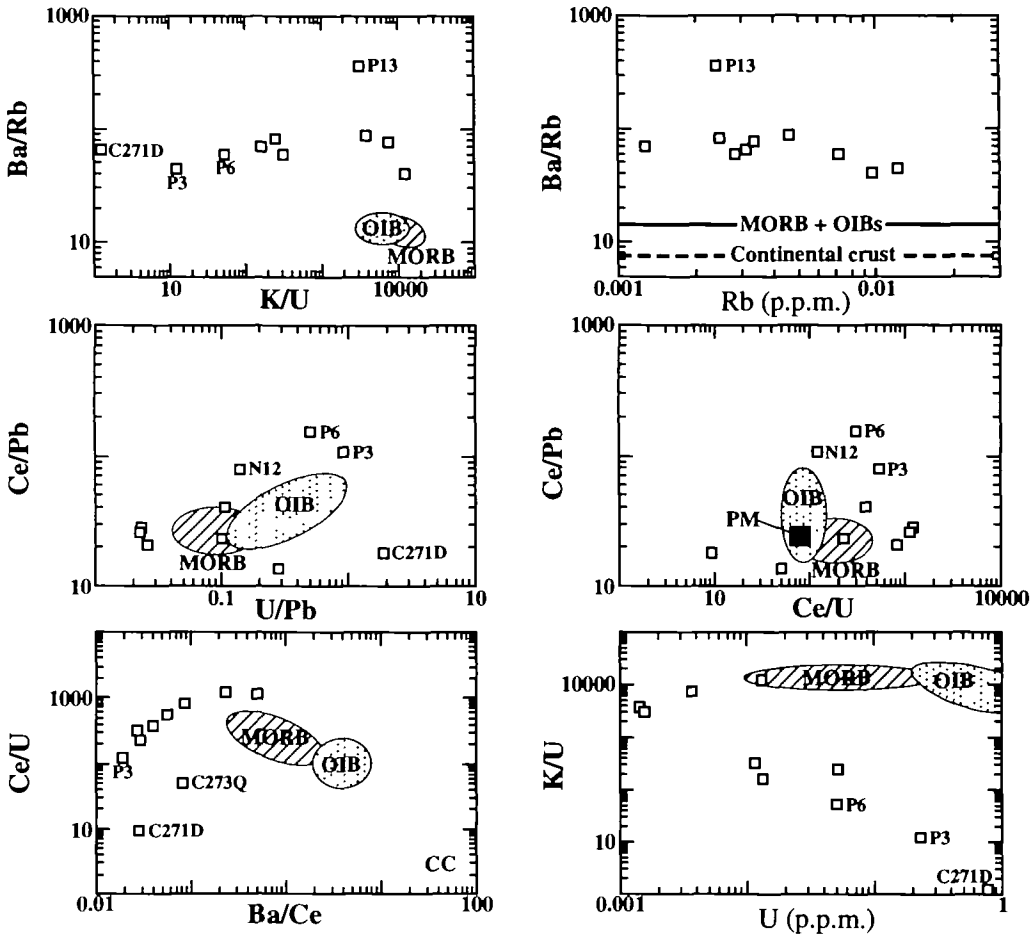

Fig. 6. Plots of trace element concentrations and ratios of clinopyroxenes. CC—continental crust.

pared with more recent mineral picking. Both samples C271I and P12 yield similar orthopyroxene–clinopyroxene partition coefficients for REE and Rb, but different values for K and Sr. This variability in partition coefficients is independent of the absolute concentrations of these elements in the clinopyroxenes. The orthopyroxene–clinopyroxene partition coefficients for REE display gradual increases with increasing atomic number, despite the difference in REE patterns of clinopyroxenes between these two samples. Petrographically, the amphibole of P6 seems to be in chemical equilibrium with coexisting clinopyroxene. All the amphibole–clinopyroxene partition coefficients exceed unity except for U, which is close to unity. These results are similar to those of O'Reilly *et al.* (1991). The amphibole–clinopyroxene partition coefficients for REE are very constant at ~1·2, but, as expected, the partition coefficients of garnet–clinopyroxene indicate that K and HREE (Dy to Lu) tend to concentrate in garnet, whereas U, Pb, Sr and LREE are excluded less by clinopyroxene.

Isotopic compositions

The ε_{Nd} of clinopyroxene from the xenoliths, megacrysts (Table 6) and the basaltic lavas from the Cameroon line are plotted in Fig. 7, where the lavas are divided into oceanic sector, continent–ocean boundary (c.o.b.) and the continental sector (Halliday *et al.*, 1990). Megacrysts have the same range of ε_{Nd} as the basaltic lavas from the oceanic and the continental sectors, except sample C201D, which has an ε_{Nd} similar to the c.o.b. lavas with slightly lower ε_{Nd}. C201D was collected from Mt Cameroon, which is part of the c.o.b. and thus explains its ε_{Nd}. The similarity in ε_{Nd} between the megacrysts and the Cameroon line lavas strongly suggests a genetic relationship between the Cameroon line magmas and the megacrysts, but not necessarily the host magmas in which they were entrained. A cogenetic relationship between megacrysts and their host magmas has been advocated by some others (Kramers *et al.*, 1983; Irving & Frey, 1984; Menzies *et al.*, 1985; Erlank *et al.*, 1987), but criticized by

Table 6: Isotopic and trace element ratios

Sample:	Rock type	Mineral	$^{87}Sr/^{86}Sr$ ± 2σ errors	$^{143}Nd/^{144}Nd$ ± 2σ errors	ε_{Nd}	$^{206}Pb/^{204}Pb$	$^{207}Pb/^{204}Pb$	$^{208}Pb/^{204}Pb$	$^{87}Rb/^{86}Sr$	$^{147}Sm/^{144}Nd$	$^{238}U/^{204}Pb$	T_{DM} (Ma)
Xenoliths												
C235A	sp lherz	cpx	0·702369±8	0·513287±5	+13	17·73	15·45	38·75	0·000118	0·2572	6·69	480
C235D	sp lherz	cpx	0·702560±17	0·513260±12	+12	17·90	15·49	37·62	0·000061	0·2656	6·27	320
C271D	sp lherz	cpx	0·703074±10	0·513267±7	+12	19·78	15·65	39·38	0·000272	0·3027	125	200
C271I	sp lherz	cpx	0·701749±10	0·513511±10	+17	17·78	15·21	36·73	0·000154	0·2758	1·57	880
	sp lherz	opx	0·70230±4	0·51348±14	+16	—	—	—	0·021	0·456	—	
C273Q	sp lherz	cpx	0·702650±11	0·513210±8	+11	18 19	15·63	38·03	0·000126	0·2673	17·6	170
N12	harz	cpx	0·704156±8	0·512616±6	−0·4	21·00	15·57	40·68	0·000198	0·1734	9·67	
	harz	opx	—	0·512567±12	−1·4	—	—	—	—	0·267	—	
P3	sp lherz	cpx	0·702919±10	0·513019±7	+7·4	20·13	15·67	39·99	0·000235	0·1098	60·4	190
P6	sp–gt web	cpx	0·702761±11	0·512910±7	+5·3	18·91	15·54	38·67	0·000196	0·1729	32·2	
	sp–gt web	amp	0·702974±14	0·512961±12	+6·6	18·92	15·54	38·64	0·0291	0·1747	5·84	
	sp–gt web	gt	—	0·512975±35	+6·6	19·38	15·75	38·79	0·00140	0·8175	14·3	
P12	sp–gt web	cpx	0·702293±15	0·513234±11	+12	18·13	15·51	37·58	0·000368	0·2392	1·46	
	sp–gt web	opx	0·70246±4	—	—	18·93	15 71	38·40	0·00310	0·446	—	
P13	sp lherz	cpx	0·702217±11	0·513242±9	+12	18·04	15·50	37·53	0·00019	0·2389	1·39	
Megacrysts												
C201D*	megst	cpx	0·703355±13	0·512792±8	+3·0	20·21	15·74	39·89	0·000244	0·1827	4·24	
C241	megst	fs	0·703117±13	0·512934±7	+5·8	—	—	—	0·00129	0·05496	—	
N12	megst	gt	0·709848±26	0 512870±10	+4 5	17·81	15·55	37·64	0·338	0·5874	2·34	
N12	megst	fs	0·703024±17	0·512915±8	+5·4	19·83	15·68	39·78	0·0021	0·0633	—	
N12	megst	cpx	0·70334±4	0·512903±7	+5·2	20·46	15·79	40·52	0·000945	0·2104	8·09	
N30	megst	cpx	0·703108±11	0·512966±8	+6·4	—	—	—	0·000091	0·2031	—	

Megst, megacryst; sp lherz, spinel lherzolite; harz, harzburgite; sp–gt web, spinel–garnet websterite; cpx, clinopyroxene; opx, orthopyroxene; gt, garnet; amp, amphibole; fs, feldspar.
*The isotopic compositions of C201D were taken from Halliday *et al.* (1990).
All isotopic compositions and parent/daughter ratios are blank corrected. The uncertainties of $^{87}Rb/^{86}Sr$, $^{147}Sm/^{144}Nd$ and $^{238}U/^{204}Pb$ are estimated to be 1%, 0·5% and 2%, respectively.

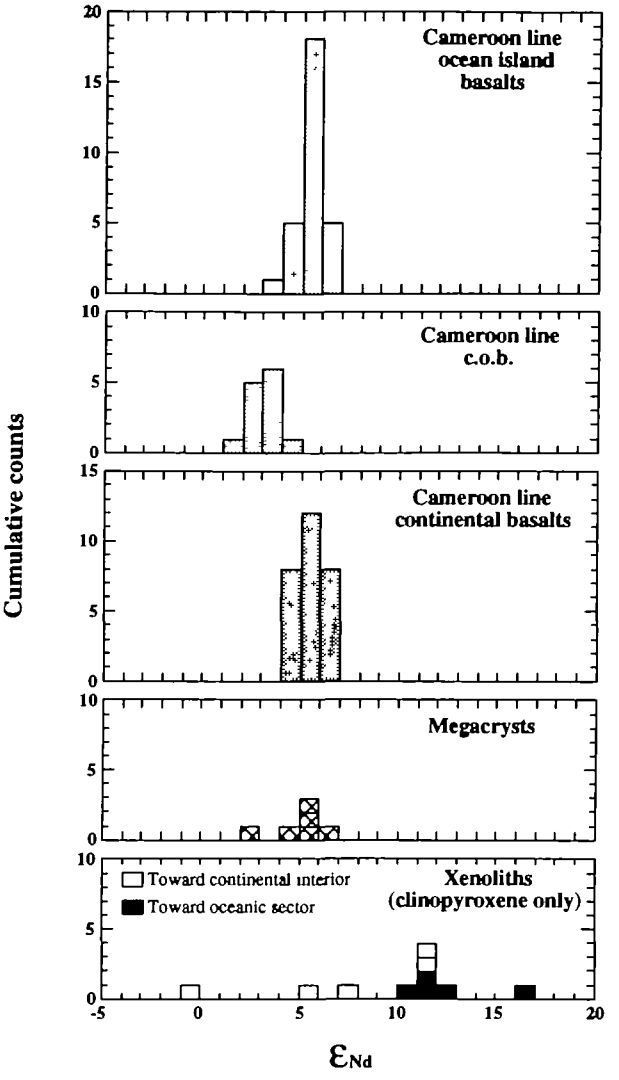

Fig. 7. Histogram of ε_{Nd} for the clinopyroxenes from xenoliths, megacrysts and basic lavas from the oceanic, continent–ocean boundary (c.o.b.) and continental sector of the Cameroon line (Halliday *et al.*, 1988, 1990; Lee, 1994; Lee *et al.*, 1994).

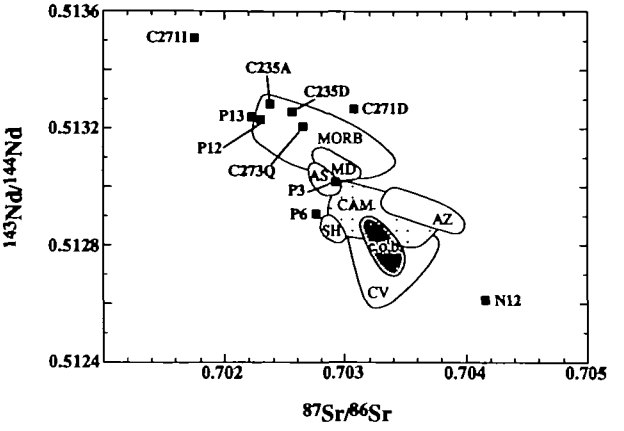

Fig. 8. Plot of $^{87}Sr/^{86}Sr$ vs $^{143}Nd/^{144}Nd$ of the clinopyroxenes in this study. Also included are Atlantic N-MORB (Newsom *et al.*, 1986), Cape Verdes (CV; Davies *et al.*, 1989), St. Helena [SH; White & Hofmann (1982)], Ascension, (AS) Azores (AZ) and Madeira (MD) [all from Halliday *et al.* (1992)], Cameroon line OIBs (CAM) and c.o.b. (Halliday *et al.*, 1988, 1990; Lee, 1994; Lee *et al.*, 1994).

others (Shimizu & Richardson, 1987). In contrast, the xenoliths display larger variations in ε_{Nd} from −1 to +17 (Table 6). Xenoliths from the continental interior are systematically lower in ε_{Nd} (Fig. 7).

The isotopic compositions of Sr and Nd for clinopyroxenes are plotted in Fig. 8, along with various ocean island basalts (OIB) for reference. The xenoliths cover a large range of isotopic compositions from depleted to near Bulk Earth. The spinel lherzolites with LREE depletions are characterized by depleted isotopic compositions, and are comparable with or more depleted than the Atlantic N-MORB. The two samples that contain trace amphibole and U and LREE enrichments (C271D and P3) have Sr isotopic compositions comparable with the Cameroon line lavas. The Nd isotopic compositions of these two samples, however, are correlated with their Sm/Nd ratios. Sample P3 has relatively lower Sm/Nd (Fig. 4), and plots close to the Cameroon line lavas. In contrast, C271D has a higher Sm/Nd and exhibits an Nd isotopic composition comparable with that of Atlantic N-MORB. The amphibole websterite (P6) plots close to the field of the Cameroon line lavas. The harzburgite (N12) exhibits slightly enriched Sr and Nd isotopic compositions close to Bulk Earth, differing from the rest of the Cameroon line xenoliths and the host lavas. The three samples with the least radiogenic Nd, N12, P3 and P6, all have distinctly higher Ce/Pb (78–155, compared with 14–40 for the rest of the xenoliths). This supports the view that the trace element compositions reflect the age of the lithospheric mantle, and provides clear evidence that increases in Ce/Pb are related to a long-term history of source LREE enrichment (Halliday *et al.*, 1995). It should be noted that this is consistent with enrichment of the continental lithosphere by OIB-like melts (Brooks *et al.*, 1976; Paslick *et al.*, 1995). There is no evidence for enrichment from subduction-related components with low Ce/Pb (Miller *et al.*, 1994).

As with the Sr and Nd data, Pb isotopic compositions of the clinopyroxenes cover a large range (Fig. 9). The LREE-depleted lherzolites and the two samples with concave-downward REE patterns, P12 and P13, have the most unradiogenic Pb isotopic compositions, plotting to the left or within the field of the Atlantic N-MORB (Fig. 9). The two LREE-enriched lherzolites, C271D and P3 (with high

$^{238}U/^{204}Pb$, μ, values of 125 and 60, respectively), plot close to the field of the Cameroon line lavas. Given the measured μ values, both amphibole-bearing lherzolites have 'relatively' unradiogenic $^{207}Pb/^{204}Pb$ ratios, consistent with a 'relatively' recent U/Pb enrichment in the sources (Halliday *et al.*, 1990, 1992, 1995). Amphibole-bearing websterite P6 has Pb isotopic compositions intermediate between those of LREE-depleted and LREE-enriched lherzolites, lying close to the field of the Cameroon line lavas. Harzburgite N12 records the highest $^{206}Pb/^{204}Pb$ (21·0) and $^{208}Pb/^{204}Pb$ (40·4) ratios in this study. However, this is distinct from HIMU and any other typical mantle component if one considers $^{207}Pb/^{204}Pb$, $^{87}Sr/^{86}Sr$ and $^{143}Nd/^{144}Nd$.

Although the differences in isotopic compositions (particularly Pb) are substantial among different volcanic centers, there is no systematic relationship between geography and isotopic compositions for the xenoliths. The variations in $^{87}Sr/^{86}Sr$ for xenoliths within individual volcanic centers are minor, e.g. 0·70222–0·70229 for Ngaoundéré plateau and 0·70237–0·70256 for Mt Cameroon, implying localized homogeneity of the lithosphere.

Clinopyroxene data are also plotted on conventional Sm–Nd and U–Pb isochron diagrams (Fig. 10). The $^{143}Nd/^{144}Nd$ of clinopyroxenes are positively correlated with $^{147}Sm/^{144}Nd$ corresponding to an age of 460 Ma. Xenoliths from this study have lower Sm/Nd ratios than abyssal peridotites (Johnson *et al.*, 1990), consistent with the xenoliths representing a potential MORB source for the local mantle, rather than residues of recent MORB extraction. The majority of the clinopyroxenes have μ values <10, yet the clinopyroxenes for those xenoliths containing amphibole have μ values up to 125 (C271D). Consequently, two samples from within the same volcanic center have very different μ values, 1·6 and 125. Halliday *et al.* (1990) suggested that a U/Pb fractionation and enrichment occurred in the Cameroon line upper mantle at ~125 Ma. High μ (>10) xenoliths yield Pb isotopic compositions consistent with such Mesozoic enrichments of the source (Fig. 10). Such enrichments find no parallel in the volcanism of the Cameroon line (Fitton,

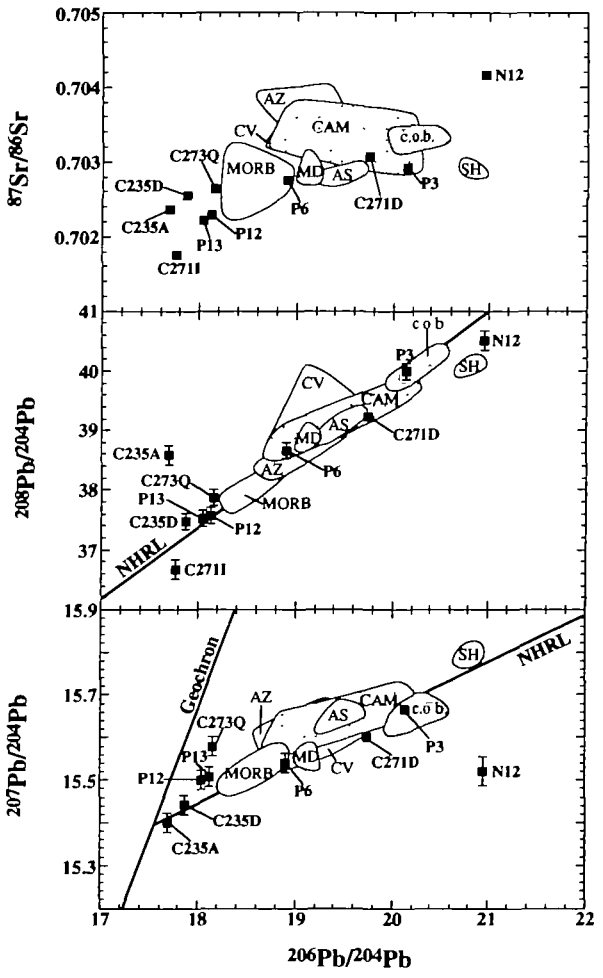

Fig. 9. Plots of $^{206}Pb/^{204}Pb$ vs $^{207}Pb/^{204}Pb$, $^{208}Pb/^{204}Pb$ and $^{87}Sr/^{86}$ for the clinopyroxenes. Reference fields are from the sources listed in Fig. 8.

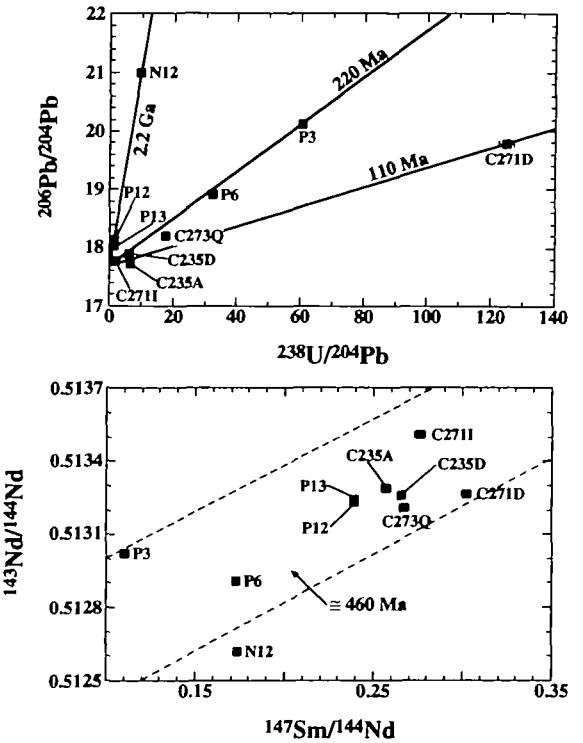

Fig. 10. Conventional Sm–Nd and U–Pb isochron diagrams for the clinopyroxenes.

1987), which was probably triggered by a deep mantle plume that produced melts that interacted with this previously enriched mantle (Lee *et al.*, 1994). However, the timing and long-term isotopic effects of such Mesozoic enrichment appear to be similar in the xenoliths and the source regions of the Cameroon line magmas.

The Nd model ages (relative to depleted mantle, DM) for the clinopyroxenes with Sm/Nd that differ from depleted mantle or Bulk Earth, vary from late Proterozoic to Mesozoic (880–170 Ma; Table 4). For rocks having low ε_{Nd} relative to depleted mantle, a late decrease in Sm/Nd (addition of LREE-enriched partial melts) tends to lower their model ages. Similarly, for rocks that have high ε_{Nd} relative to depleted mantle, a late increase in Sm/Nd (extraction of partial melts) will also lower their model ages. Therefore, it is significant that the three samples with high U/Pb and Sm/Nd ≠ Bulk Earth or depleted mantle all yield young t_{DM} model ages (Table 4), even though only P3 is LREE enriched with $\varepsilon_{Nd} <$ DM. This is consistent with U/Pb fractionation–enrichment in the Mesozoic, concomitant with both extraction (C273Q) and addition (P3) of partial melts in the lithospheric mantle. The mantle represented by C271D must have experienced both processes, and the enrichment probably took place shortly after the extraction of partial melts (Fig. 4)

Inter-mineral isotopic equilibrium

Orthopyroxenes from both C271I and P12 and the amphibole of P6 all have higher $^{87}Sr/^{86}Sr$ than that of coexisting clinopyroxene (Fig. 11). Even though all three mineral pairs demonstrate positive correlations between $^{87}Rb/^{86}Sr$ and $^{87}Sr/^{86}Sr$, there are concerns about interpreting the variations in $^{87}Sr/^{86}Sr$ as reflecting radiogenic ingrowth. It is no surprise that orthopyroxene is more susceptible to contamination in the mantle, by fluids or melt, than clinopyroxene because of its lower Sr concentrations. In addition, the inter-mineral $^{87}Sr/^{86}Sr$ variations are no larger than inter-xenolith $^{87}Sr/^{86}Sr$ variations of clinopyroxenes from the same outcrop, e.g. C235A vs C235D and C271I vs C271D. The clinopyroxenes are unlikely to be contaminated to any significant extent, given the unradiogenic Sr, the very low Rb/Sr and the uniform but non-basaltic Ba/Rb.

Convincing evidence of isotopic equilibration is found in the Nd. The clinopyroxene and orthopyroxene of C271I have similar Nd isotopic compositions that are within analytical uncertainty, whereas their $^{147}Sm/^{144}Nd$ ratios show significant differences (Fig. 11). Similarly, the clinopyroxene, amphibole and garnet of P6 also show isotopic equilibration in Nd but display significant variations in $^{147}Sm/^{144}Nd$ by up to a factor of four (Fig. 11). The lack of inter-mineral difference in $^{143}Nd/^{144}Nd$ suggests that the Nd isotopic compositions in C271I and P6 have been reset recently, or that the xenoliths recently cooled below the blocking temperature for Nd in garnet (600–650°C; Mezger *et al.*, 1992). In contrast, the two pyroxenes of N12 show minor differences in $^{143}Nd/^{144}Nd$. This could be attributed to small blank contributions (≤0·1%) to the orthopyroxene. Alternatively, it is possible that the two pyroxenes of N12 were not in isotopic equilibrium given that the orthopyroxene is porphyroblastic in contrast to smaller (< 1 mm) and interstitial clinopyroxene. The clinopyroxene and amphibole from P6 have similar $^{206}Pb/^{204}Pb$ despite a huge difference in μ suggesting recent equilibration, whereas garnet has more radiogenic $^{206}Pb/^{204}Pb$ and intermediate μ (Table 6). The amphibole–clinopyroxene equilibrium implies recent equilibration of Pb between these phases. The radiogenic Pb in the garnet of P6 might reflect the very high closure temperature of Pb in this phase (Mezger *et al.*, 1992; Burton *et al.*, 1995). This being the case, the 'age' calculated is ~340 Ma, and defines the time of garnet growth or the last time that this portion of the lithosphere cooled through ≥900°C (Burton *et al.*, 1995). These data

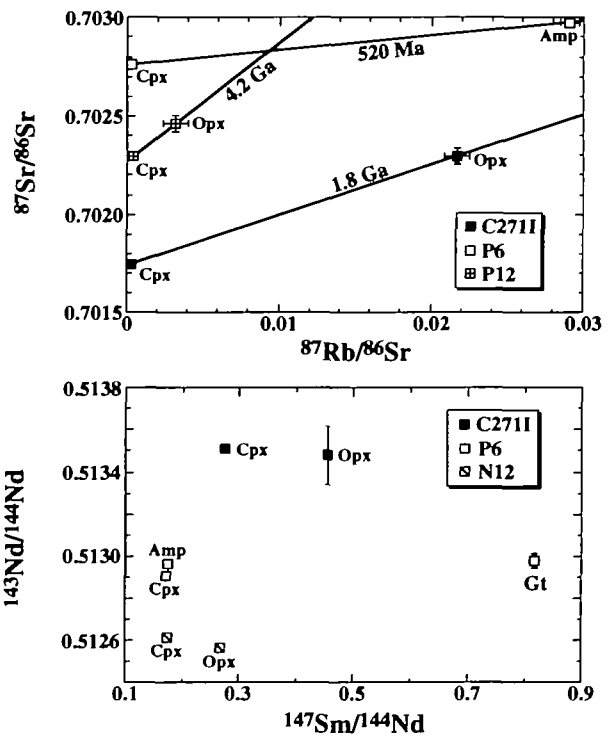

Fig. 11. Plots of inter-mineral isotopic variations in Rb–Sr and Sm–Nd isotope systems.

combined with the Sm–Nd equilibration imply that the upper portion of the sub-continental lithosphere has remained at $\geqslant 600°C$ for several hundred million years.

Origin of megacrysts

Six megacrysts, three of clinopyroxene, two feldspar and one garnet, have been analyzed in this study [one from Mt Cameroon (C201D), one from Bambouto (C241) and four from Biu Plateau (N12 and N30); Fig. 1]. All three clinopyroxenes display depletions in both LREE and HREE with concave-downward patterns (Fig. 4f). The more significant depletion of HREE vs LREE in each sample probably reflects the presence of garnet during crystallization. The REE patterns of the feldspar (fs) and the garnet are typical of fractional crystallization products, LREE enriched with positive Eu anomalies for the feldspar and HREE enriched for the garnet. Three megacrysts of N12 are from the same lava flow. Despite the presence of a positive Eu anomaly in the feldspar, neither clinopyroxene nor garnet shows a deficit in Eu, which indicates they are genetically unrelated or the feldspar grew after the other phases. All the megacrysts included in this study have similar Nd isotopic compositions to the Cameroon line lavas, in favor of the megacrysts having precipitated from magmas genetically linked with the Cameroon line lavas (Fig. 9).

Although the Nd isotopic composition of the garnet megacryst is no different from that of the Cameroon line lavas, its Sr and Pb isotopic compositions are comparable with lower-crustal xenoliths of the Cameroon line (Fig. 12; Halliday *et al.*, 1988). This is explicable if the megacrysts grew by fractional crystallization from earlier underplated Cameroon line lavas while assimilating the lower continental crust. Although the Sr and Pb in the garnet were affected by continental contributions, the Nd retained the signature of the Cameroon line lavas, indicating that Nd is less susceptible to contamination. Consequently, these data provide little meaningful age information, as the isotopic variations do not reflect *in situ* radioactive decay. Crustal assimilation is also documented in some basaltic lavas from Bambouto and Oku areas and in the majority of the evolved rocks from the Cameroon line (Lee, 1994).

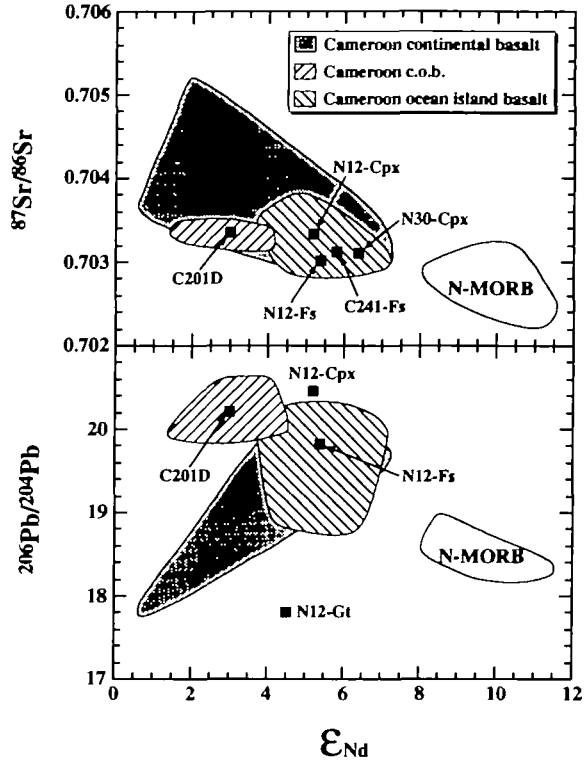

Fig. 12. Plots of ε_{Nd} vs $^{87}Sr/^{86}Sr$ and $^{206}Pb/^{204}Pb$ of the megacrysts, Cameroon line ocean island basalts, c.o.b. and continental basalts, and Atlantic N-MORB.

DISCUSSION AND CONCLUSIONS

Although the variations in major element chemistry of the Cameroon line xenoliths can be ascribed simply to partial melt extraction, the incompatible trace element and isotopic compositions of these samples imply multi-stage depletions and metasomatic enrichments. It has been previously noted that fertile peridotites, high in Al_2O_3 and CaO, essential components of basalt, are generally LREE depleted whereas infertile peridotites are often LREE enriched, i.e. the degree of LREE depletion increases with Al_2O_3 in the xenolith (Frey & Green, 1974; Frey, 1984; Stosch *et al.*, 1986; Kempton, 1987; O'Reilly & Griffin, 1988; Zindler & Jagoutz, 1988; Galer & O'Nions, 1989). This is the opposite of that predicted by a conventional partial melting model. The observed differences between major and trace elements are usually attributed to either: (1) mixing between a partial melting residue that dominates the major element chemistry and a second component that controls the bulk of the incompatible trace elements (Frey & Green, 1974; Frey & Prinz, 1978; Song & Frey, 1989); or (2) partial melting and metasomatism occurring concurrently in magma conduits (Galer & O'Nions, 1989). Although it is not required, the first scenario favors a lithospheric mantle that is partly stratified, with fertile peridotites at the base and infertile peridotites and harzburgites on top. The idea of stratified mantle finds supports from ocean ridge melting models

(McKenzie, 1985) and studies of xenolith suites world-wide (Irving, 1980; Griffin *et al.*, 1984; Kempton *et al.*, 1984; Menzies *et al.*, 1985; O'Reilly & Griffin, 1985; Kempton, 1987; Nielson & Noller, 1987). The second model explains the coupling of metasomatic enrichment and infertile lherzolites by interactions between the depleted lherzolites and locally derived magmas (Galer & O'Nions, 1989). Thus, host magmas and the metasomatized xenoliths should have roughly the same isotopic compositions if the second model is correct.

The relationship between La/Nd in clinopyroxene, an indication of LREE depletion, and Al_2O_3 contents in spinel is illustrated in Fig. 13. The samples from the Cameroon line show an overall negative correlation, with the majority of the anhydrous lherzolites plotting to the lower right. This trend is defined mainly by C271D and P3; the remaining samples display a positive correlation not normally found in xenoliths (Frey & Green, 1974; Frey & Prinz, 1978; Song & Frey, 1989), but typical of many peridotite massifs (e.g. Pearson *et al.*, 1993). This positive correlation between major and trace element chemistry in the ultramafic xenoliths is consistent with that predicted with a basaltic melt extraction model: the more fertile the lherzolite the less depleted the LREE. This implies that the metasomatism of C271D, P3 and P6 is distinct from the main depletion of the anhydrous peridotites in this study, and these anhydrous peridotites probably record the lithospheric mantle compositions associated with the most recent crust-forming events (Late Proterozoic).

Amphibole can be stable throughout the stability field of spinel lherzolite at $T \leqslant 1050°C$ (Jenkins, 1983; Olafsson & Eggler, 1983), and is frequently associated with LREE enrichment in metasomatized ultramafic xenoliths (Menzies & Murthy, 1980; Stosch *et al.*, 1980; Menzies, 1983; Neal, 1988; Stolz & Davies, 1988). Metasomatism provides LREE to the peridotites along with volatiles to form amphibole. Pargasitic amphibole appears as a trace mineral phase in the two LREE-enriched lherzolites, C271D and P3, and as a major mineral phase in P6, which lack LREE enrichment.

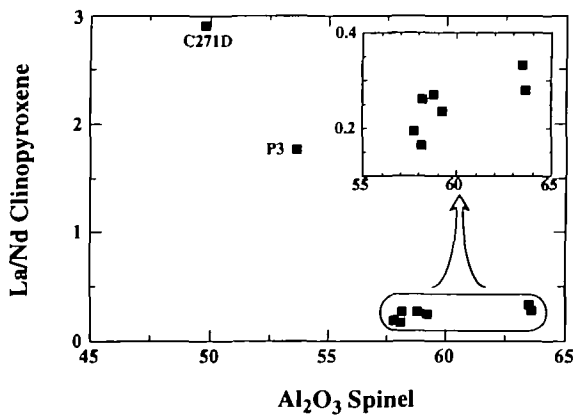

Fig. 13. Plot of Al_2O_3 in spinel vs La/Nd ratios for the clinopyroxene, which indicates the depletion of light rare earth elements.

The amphiboles in C271D and P3 are associated with Mesozoic enrichments, similar to those that are recorded in the source regions of later Cameroon line magmatism. Both C271D and P3 have Sr and Pb isotopic compositions similar to those of the Cameroon line lavas (Fig. 9), whereas unmetasomatized lherzolites, e.g. C271I and P13, have significantly more depleted isotopic compositions. The Nd isotopic compositions of the metasomatized xenoliths, however, are more radiogenic than the host lavas. Furthermore, a mass balance calculation suggests that compared with the depleted xenoliths (e.g. C235) the metasomatic component must have had an La/Nd ratio between 2·8 and 3·2. This calculated component is significantly more LREE enriched than any of the Cameroon line lavas, which have La/Nd ratios in the range of 0·7–1·7 (Fitton, 1987).

The Nd model ages of LREE depleted spinel lherzolites (C235A, C235D and C271I) range from Paleozoic to late Proterozoic (Table 4). These model ages probably reflect events of crustal formation. In contrast, the U–Pb data (Fig. 10) seem to indicate some U enrichments occurred in the Mesozoic, and all three U-enriched lherzolites (P3, C271D and C273Q) yield similar Mesozoic Nd model ages (Table 4). Such enrichment events are supported by the Pb isotope data for the Cameroon line basaltic lavas (Halliday *et al.*, 1990), and are consistent with formation during a major thermal event associated with the opening of the Atlantic Ocean in the Mesozoic. The inter-mineral Nd isotopic equilibrium observed in P6 (Fig. 11) also indicates that the metasomatism happened sufficiently long ago that the minerals subsequently reached chemical and isotopic equilibrium. These constraints demonstrate that the depletion and enrichment observed in the Cameroon line xenoliths cannot have occurred concurrently (Figs 8 and 10), and argue against the model of simultaneous melt extraction and contamination (Galer & O'Nions, 1989). None the less, the Nd model ages suggest that U/Pb enrichment was accompanied by either Sm/Nd depletion or enrichment such that on a local scale the model of Galer & O'Nions (1989) may be upheld. These xenoliths may represent fragments of sub-continental lithosphere that formed at about the same time as the last major crust-forming event, the Pan-African,

and were subsequently enriched by small melt fractions percolating through the upper mantle at the time of early break-up of Pangea. The passage of small melt fractions also produced the concomitant trace element enrichment in the sources of the Cameroon line basaltic lavas (Halliday *et al.*, 1990).

ACKNOWLEDGEMENTS

Comments by M. Gurnis, M. Menzies, S. Mukasa, J. Rosenbaum and an anonymous reviewer are greatly appreciated. C. Hall, M. Johnson and R. Keller are thanked for their technical assistance. This research was supported by NSF Grants EAR 89-15936 and EAR 92-05435 to A. N. Halliday.

REFERENCES

Adam, J., Green, T. H. & Day, R. A., 1992. An experimental study of two garnet pyroxenite xenoliths from the Bullenmerri and Gnotuk Maars of western Victoria, Australia. *Contributions to Mineralogy and Petrology* **111,** 505–514.

Allègre, C. J., 1982. Chemical geodynamics. *Tectonophysics* **81,** 109–132.

Allègre, C. J., Dupré, B., Lambert, B. & Richard, P., 1981. The subcontinental versus suboceanic debate, I. Lead–neodymium–strontium isotope in primary alkali basalts from a shield area: the Ahaggar volcanic suite. *Earth and Planetary Science Letters* **52,** 85–92.

Altherr, R., Henjes-Kunst, F. & Baumann, A., 1990. Asthenosphere versus lithosphere as possible sources for basaltic erupted during formation of the Red Sea: constraints from Sr, Pb and Nd isotopes. *Earth and Planetary Science Letters* **96,** 269–286.

Andersen, T., O'Reilly, S. Y. & Griffin, W. L., 1984. The trapped fluid phase in the upper mantle xenoliths from Victoria: implications for mantle metasomatism. *Contributions to Mineralogy and Petrology* **88,** 72–85.

Basu, A. R. & Murthy, V. R., 1977. Ancient lithospheric lherzolite xenolith in alkali basalt from Baja California. *Earth and Planetary Science Letters* **35,** 239–246.

Beeson, M. H. & Jackson, E. D., 1970. Origin of garnet pyroxenite xenoliths at Salt Lake Crater, Oahu. *Mineralogical Society of America, Special Paper* **3,** 95–112.

Brey, G. P. & Köhler, T. P., 1990. Geothermobarometry in natural four-phase lherzolites II. New thermometers, and practical assessment of existing thermobarometers. *Journal of Petrology* **31,** 1353–1379.

Brooks, C., James, D. E. & Hart, S. R., 1976. Ancient lithosphere: its role in young continental volcanism. *Science* **193,** 1086–1984.

Burns, R. G., 1969. Site preference of transition metal ions in silicate crystal structures. *Chemical Geology* **5,** 275–283.

Burns, R. G., 1970. *Mineralogical Applications of Crystal Field Theory.* Cambridge: Cambridge University Press.

Burton, K. W., Kohn, M. J., Cohen, A. S. & O'Nions, R. K., 1995. The relative diffusion of Pb, Nd, Sr and O in garnet. *Earth and Planetary Science Letters* **133,** 199–211.

Dasch, J. E. & Green, D. H., 1975. Strontium isotope geochemistry of lherzolite inclusions and host basaltic rocks, Victoria, Australia. *American Journal of Science* **275,** 461–469.

Davies, G. R., Norry, M. J., Gerlach, D. C. & Cliff, R. A., 1989. A combined chemical and Pb–Sr–Nd isotope study of the Azores and Cape Verde hotspots: the geodynamic implications. In: Saunders, A. D. & Norry, M. J. (eds) *Magmatism in the Ocean Basins. Geological Society of London, Special Publication* **42,** 231–255.

Dawson, J. B., 1982. Contrasting types of mantle metasomatism. *Terra Cognita* **2,** 232–233.

Déruelle, B., Moreau, C., Nkoumbou, C., Kambou, R., Lissom, J., Njonfang, E., Ghogomu, R. T. & Nono, A., 1991. The Cameroon line: a review. In: Kampunzu, A. B. & Lubala, R. T. (eds) *Magmatism in Extensional Structure Settings: the Phanerozoic African Plate.* Berlin: Springer-Verlag, pp. 275–327.

Dorbath, C., Dorbath, L., Fairhead, J. D. & Stuart, G. W., 1986. A teleseismic delay time study across the Central African Shear Zone in the Adamawa region of Cameroon, West Africa. *Geophysical Journal of the Royal Astronomical Society* **86,** 751–766.

Dupuy, C., Barsczus, H. G., Liotard, J.-M. & Dostal, J., 1988. Trace element evidence for the origin of ocean island basalts: an example from the Austral Islands. *Contributions to Mineralogy and Petrology* **98,** 293–302.

Ellis, D. J. & Green, D. H., 1979. An experimental study of the effect of Ca upon garnet–clinopyroxene Fe–Mg exchange equilibria. *Contributions to Mineralogy and Petrology* **71,** 13–22.

Emery, K. O. & Uchupi, E., 1984. *The Geology of the Atlantic Ocean.* New York: Springer.

Erlank, A. J., Waters, F. G., Hawkesworth, C. J., Haggerty, S. E., Allsopp, H. L., Richard, R. S. & Menzies, M. A., 1987. Evidence for mantle metasomatism in peridotite nodules from Kimberley pipes, South Africa. In: Menzies, M. A. & Hawkesworth, C. J. (eds) *Mantle Metasomatism.* London: Academic Press, pp. 221–311.

Fitton, J. G., 1987. The Cameroon line, West Africa: a comparison between oceanic and continental alkaline volcanism. In: Fitton, J. G. & Upton, B. G. J. (eds) *Alkaline Igneous Rocks. Geological Society of London, Special Publication* **30,** 273–291.

Fitton, J. G. & Dunlop, H. M., 1985. The Cameroon line, West Africa, and its bearing on the origin of oceanic and continental alkali basalt. *Earth and Planetary Science Letters* **72,** 23–38.

Fitton, J. G., Kilburn, C. R. J., Thirlwall, M. F. & Hughes, D. J., 1983. 1982 eruption of Mt. Cameroon, West Africa. *Nature* **306,** 327–332.

Freeth, S. J., 1979. Deformation of the African plate as a consequence of membrane stress domains generated by post-Jurassic drift. *Earth and Planetary Science Letters* **45,** 93–104.

Frey, F. A., 1984. Rare earth abundances in upper mantle rocks. In: Henderson, P. (ed.) *Rare Earth Element Geochemistry.* Amsterdam: Elsevier, pp. 153–203.

Frey, F. A. & Green, D. H., 1974. The mineralogy, geochemistry and origin of lherzolite inclusions in Victorian basanites. *Geochimica et Cosmochimica Acta* **38,** 1023–1059.

Frey, F. A. & Prinz, M., 1978. Ultramafic inclusions from San Carlos, Arizona: petrologic and geochemical data bearing on their petrogenesis. *Earth and Planetary Science Letters* **38,** 129–176.

Frey, F. A. & Roden, M. F., 1987. The mantle source for the Hawaiian Islands: constraints from the lavas and ultramafic inclusions. In: Menzies, M. A. & Hawkesworth, C. J. (eds) *Mantle Metasomatism.* London: Academic Press, pp. 422–463.

Galer, S. J. G. & O'Nions, R. K., 1989. Chemical and isotopic studies of ultramafic inclusions from the San Carlos Volcanic Field, Arizona: a bearing on their petrogenesis. *Journal of Petrology* **30,** 1033–1064.

Green, D. H., 1966. The origin of the 'eclogites' from Salt Lake Crater, Hawaii. *Earth and Planetary Science Letters* **1,** 414–420.

Green, T. H. & Adam, J., 1991. Assessment of the garnet–clinopyroxene Fe–Mg thermometer using new experimental data. *Journal of Metamorphic Geology* **9**, 341–347.

Griffin, W. L., Wass, S. Y. & Hollis, J. D., 1984. Ultramafic xenoliths from Bullenmerri and Gnotuk maars, Victoria, Australia: petrology of a subcontinental crust–mantle transition. *Journal of Petrology* **25**, 53–78.

Halliday, A. N., Dickin, A. P., Fallick, A. E. & Fitton, J. G., 1988. Mantle dynamics: a Nd, Sr, Pb and O isotopic study of the Cameroon line volcanic chain. *Journal of Petrology* **29**, 181–211.

Halliday, A. N., Davidson, J. P., Holden, P., DeWolf, C. P., Lee, D.-C. & Fitton, J. G., 1990. Trace-element fractionation in plume and the origin of HIMU mantle beneath the Cameroon line. *Nature* **347**, 523–528.

Halliday, A. N., Davies, G. R., Lee, D.-C., Tommasini, S., Paslick, C. R., Fitton, J. G. & James, D. E , 1992. Lead isotope evidence for young trace element enrichment in the oceanic upper mantle. *Nature* **359**, 623–627. (Correction. 1993, *Nature* **362**, 184.)

Halliday, A. N., Lee, D.-C., Tommasini, S., Davies, G. R., Paslick, C. R., Fitton, J. G. & James, D. E., 1995. Incompatible trace elements in OIB and MORB and source enrichment in the sub-oceanic mantle. *Earth and Planetary Science Letters* **133**, 379–395.

Hamelin, B. & Allègre, C. J., 1988. Lead isotope study of orogenic lherzolite massifs. *Earth and Planetary Science Letters* **91**, 112–131.

Hanson, G. N., 1977. Geochemical evolution of the suboceanic mantle. *Journal of Geological Society of London* **134**, 235.

Hanson, G. N., 1980. Rare earth elements in petrogenetic studies of igneous systems. *Annual Review of Earth and Planetary Sciences* **8**, 371–406.

Harley, S. L., 1984. Comparison of the garnet–orthopyroxene geobarometer with recent experimental studies, and applications to natural assemblages. *Journal of Petrology* **25**, 697–712.

Hawkesworth, C. J., Mantovani, M. S. M. & Peate, D., 1988. Lithospheric demobilization during Parana CFB magmatism. *Journal of Petrology, Special Lithosphere Issue*, 205–223.

Hervig, R. L. & Smith, J. V., 1980. Sodium thermometer for pyroxenes in garnet and spinel lherzolites. *Journal of Geology* **88**, 337–342.

Hofmann, A. W. & White, W. M., 1983. Ba, Rb and Cs in the Earth's mantle. *Zeitung für Naturforschung* **38a**, 256–266.

Hofmann, A. W., Jochum, K. P., Seufert, M. & White, W. M., 1986. Nb and Pb in oceanic basalts: new constraints on mantle evolution. *Earth and Planetary Science Letters* **79**, 33–45.

Irving, A. J., 1974. Geochemical and high pressure experimental studies of garnet pyroxenite and pyroxene granulite xenoliths from the Delegate basaltic pipes, Australia. *Journal of Petrology* **15**, 1–40.

Irving, A. J., 1980. Petrology and geochemistry of composite ultramafic xenoliths in alkali basalts and implications for magmatic processes within the mantle. *American Journal of Science* **280A**, 389–426.

Irving, A. J. & Frey, F. A., 1984. Trace element abundances in megacrysts and their host basalts: constraints on partition coefficients and megacryst genesis. *Geochimica et Cosmochimica Acta* **48**, 1201–1221.

Jenkins, D. M., 1983. Stability and composition relations of calcic amphiboles in ultramafic rocks. *Contributions to Mineralogy and Petrology* **83**, 375–384.

Jochum, K. P., Seufert, H. M., Spettel, B. & Palme, H., 1986. The solar-system abundances of Nb, Ta and Y and the relative abundances of refractory lithophile elements in differentiated planetary bodies. *Geochimica et Cosmochimica Acta* **50**, 1173–1183.

Johnson, K. T., Dick, H. J. B. & Shimizu, N., 1990. Melting in the oceanic mantle: an ion microprobe study of diopsides in abyssal peridotites. *Journal of Geophysical Research* **95**, 2661–2678.

Kempton, P. D., 1987. Mineralogic and geochemical evidence for different styles of metasomatism in spinel lherzolite xenoliths: enriched mantle source regions of basalts? In: Menzies, M. A. & Hawkesworth, C. J. (eds) *Mantle Metasomatism*. London: Academic Press, pp. 45–89.

Kempton, P. D., Menzies, M. A. & Duncan, M., 1984. Petrography, petrology and geochemistry of xenoliths and megacrysts from the Geronimo Volcanic Field, Arizona. In: Kornprobst, J. (ed.) *Kimberlites II: The Mantle and Crust–Mantle Relationships*. Amsterdam: Elsevier, pp. 71–83.

Kennedy, A. K., Lofgren, G. E. & Wasserburg, G. J., 1993. An experimental study of trace element partitioning between olivine, orthopyroxene and melt in chondrules: equilibrium values and kinetic effects. *Earth and Planetary Science Letters* **115**, 177–195.

Köhler, T. P. & Brey, G. P., 1990. Calcium exchange between olivine and clinopyroxene calibrated as a geothermobarometer for natural peridotites from 2 to 60 kb with applications. *Geochimica et Cosmochimica Acta* **54**, 2375–2388.

Kramers, J. D., Roddick, J. C. M. & Dawson, J. B., 1983. Trace element and isotope studies on veined, metasomatic and 'MARID' xenoliths from Bultfontein, South Africa. *Earth and Planetary Science Letters* **65**, 90–106.

Krogh, E. J., 1988. The garnet–clinopyroxene Fe–Mg-geothermometer—a reinterpretation of existing experimental data. *Contributions to Mineralogy and Petrology* **99**, 44–48.

Kuo, L.-C. & Essene, E. J., 1986. Petrology of spinel xenoliths from the Kishb Plateau, Saudi Arabia. *Contributions to Mineralogy and Petrology* **93**, 335–346.

Leake, B. E., 1978. Nomenclature of amphiboles. *American Mineralogist* **63**, 1023–1052.

Lee, D.-C., 1994. A chemical, isotopic and geochronological study of the Cameroon line, west Africa. Ph.D. Thesis, University of Michigan, Ann Arbor.

Lee, D.-C., Halliday, A. N., Hunter, R. H., Holden, P. & Upton, B. G. J., 1993. Rb–Sr and Sm–Nd isotopic variations in dissected crustal xenoliths. *Geochimica et Cosmochimica Acta* **57**, 219–230.

Lee, D.-C., Halliday, A. N., Fitton, J. G. & Poli, G., 1994. Isotopic variations with distance and time in the volcanic islands of the Cameroon line: evidence for a mantle plume origin. *Earth and Planetary Science Letters* **123**, 119–138.

Machado, N., Brooks, C. & Hart, S. R., 1986. Determination of initial $^{87}Sr/^{86}Sr$ and $^{143}Nd/^{144}Nd$ in primary minerals from mafic and ultramafic rocks: experimental procedure and implication for the isotopic characteristics of the Archean mantle under the Abitibi greenstone belt, Canada. *Geochimica et Cosmochimica Acta* **50**, 2335–2348.

Masuda, A., Nakamura, N. & Tanaka, T., 1973. Fine structures of mutually normalized rare-earth patterns of chondrites. *Geochimica et Cosmochimica Acta* **37**, 239–248.

McKay, G. A., 1989. Partitioning of rare earth elements between major silicate minerals and basaltic melts. In: Lipin, B. R. & McKay, G. A. (eds) *Geochemistry and Mineralogy of Rare Earth Elements. Mineralogical Society of America, Reviews in Mineralogy* **21**, 45–77.

McKenzie, D., 1985. The extraction of magma from the crust and mantle. *Earth and Planetary Science Letters* **74**, 81–91.

McKenzie, D. & O'Nions, R. K., 1983. Mantle reservoirs and ocean island basalts. *Nature* **301,** 229–231.

McKenzie, D. & O'Nions, R. K., 1991. Partial melt distributions from inversion of rare earth element concentrations. *Journal of Petrology* **32,** 1021–1091.

McKenzie, D. & O'Nions, R. K., 1995. The source regions of ocean island basalts. *Journal of Petrology* **36,** 133–159.

Menzies, M. A., 1983. Mantle ultramafic xenoliths in alkaline magmas: evidence for mantle heterogeneity modified by magmatic activity. In: Hawkesworth, C. J. & Norry, M. J. (eds) *Continental Basalts and Mantle Xenoliths*. Nantwich, UK: Shiva, pp. 92–110.

Menzies, M. A. & Murthy, V. R., 1980. Nd and Sr isotope geochemistry of hydrous mantle nodules and their host alkali basalts: implications for local heterogeneities in metasomatically veined mantle. *Earth and Planetary Science Letters* **46,** 323–334.

Menzies, M. A. & Wass, S., 1983. CO_2 rich mantle below eastern Australia: REE, Sr and Nd isotopic study of Cenozoic alkaline magmas and apatite rich xenoliths, Southern Highlands Province, New South Wales, Australia. *Earth and Planetary Science Letters* **65,** 287–302.

Menzies, M. A., Kempton, P. & Duncan, M., 1985. Interaction of continental lithosphere and asthenospheric melts below the Geronimo Volcanic Field, Arizona, USA. *Journal of Petrology* **26,** 663–693.

Menzies, M. A., Halliday, A. N., Palacz, Z., Hunter, R. H., Upton, B. G. J., Aspen, P. & Hawkesworth, C. J., 1987. Evidence from mantle xenoliths for an enriched lithospheric keel under the Outer Hebrides. *Nature* **325,** 44–47.

Mercier, J-C. C. & Nicolas, A., 1975. Textures and fabrics of upper-mantle peridotites as illustrated by xenoliths from basalts. *Journal of Petrology* **16,** 454–487.

Mezger, K., Essene, E. J. & Halliday, A. N., 1992. Closure temperatures of the Sm–Nd system in metamorphic garnets. *Earth and Planetary Science Letters* **113,** 397–409.

Miller, D. M., Goldstein, S. L. & Langmuir, C. H., 1994. Cerium/lead and lead isotope ratios in arc magmas and the enrichment of lead in the continents. *Nature* **368,** 514–520.

Moreau, C., Regnoult, J.-M., Déruelle, B. & Robineau, B., 1987. A new tectonic model for the Cameroon line, Central Africa. *Tectonophysics* **139,** 317–334.

Morgan, W. J., 1983. Hotspot tracks and the early rifting of the Atlantic. *Tectonophysics* **94,** 123–139.

Nasir, S., 1992. The lithosphere beneath the northwestern part of the Arabian plate (Jordan): evidence from xenoliths and geophysics. *Tectonophysics* **201,** 357–370.

Navon, O. & Stolper, E., 1987. Geochemical consequences of melt percolation: the upper mantle as a chromatographic column. *Journal of Geology* **95,** 285–307.

Neal, C. R., 1988. The origin and composition of metasomatic fluids and amphiboles beneath Malaita, Solomon Islands. *Journal of Petrology* **29,** 149–179.

Neumann, E.-R., 1991. Ultramafic and mafic xenoliths from Hierro, Canary Islands: evidence for melt infiltration in the upper mantle. *Contributions to Mineralogy and Petrology* **106,** 236–252.

Newsom, H. E., White, W. M., Jochum, K. P. & Hofmann, A. W., 1986. Siderophile and chalcophile element abundances in oceanic basalts, Pb isotope evolution and growth of the Earth's core. *Earth and Planetary Science Letters* **80,** 299–313.

Nickel, K. G. & Green, D. H., 1985. Empirical thermobarometry for garnet peridotites and implications for the lithosphere, kimberlites and diamonds. *Earth and Planetary Science Letters* **73,** 158–180.

Nielson, J. E. & Noller, J. S., 1987. Processes of mantle metasomatism; constraints from observations of composite peridotite xenoliths. *Geological Society of America, Special Publication* **215,** 61–76.

Olafsson, M. & Eggler, D. H , 1983. Phase relations of amphibole, amphibolite–carbonate, and phlogopite–carbonate peridotite: petrologic constraints on the asthenosphere. *Earth and Planetary Science Letters* **64,** 305–315.

O'Reilly, S. Y. & Griffin, W. L., 1985. A xenolith-derived geotherm for southeastern Australia and its geophysical implications. *Tectonophysics* **111,** 41–63.

O'Reilly, S. Y. & Griffin, W. L., 1988. Mantle metasomatism beneath western Victoria, Australia: I. Metasomatic processes in Cr-diopside lherzolites. *Geochimica et Cosmochimica Acta* 52, 433–447.

O'Reilly, S. Y., Griffin, W. L. & Ryan, C. G., 1991. Residence of trace elements in metasomatized spinel lherzolite xenolith: a proton-microprobe study. *Contributions to Mineralogy and Petrology* **109,** 98–113

Ottonello, G., 1980. Rare earth abundances and distribution in some spinel peridotite xenoliths from Assab (Ethiopia). *Geochimica et Cosmochimica Acta* **44,** 1885–1901.

Ottonello, G., Piccardo, G. B., Mazzucotelli, A. & Cimmino, F., 1978. Clinopyroxene–orthopyroxene major and rare earth elements partitioning in spinel peridotite xenoliths from Assab (Ethiopia). *Geochimica et Cosmochimica Acta* **42,** 1817–1828.

Paslick, C. R., Halliday, A. N., James, D. E. & Dawson, J. B., 1995. Enrichment of the continental lithosphere by OIB melts: isotopic evidence from the volcanic province of northern Tanzania. *Earth and Planetary Science Letters* **130,** 109–126.

Pearson, D. G., Davies, G. R. & Nixon, P. H., 1993. Geochemical constraints on the petrogenesis of diamond facies pyroxenites from the Beni Bousera peridotite massif, north Morocco. *Journal of Petrology* **34,** 125–172.

Pearson, N. J., O'Reilly, S. Y. & Griffin, W L., 1991. The granulite to eclogite transition beneath the eastern margin of the Australian craton. *European Journal of Mineralogy* **3,** 293–322.

Philpotts, J. A., Schnetzler, C. & Thomas, H. H., 1972. Petrogenetic implications of some new geochemical data on eclogitic and ultrabasic inclusions. *Geochimica et Cosmochimica Acta* **36,** 1131–1166.

Poudjom Djomani, Y. H., Diament, M. & Albouy, Y., 1992. Mechanical behavior of the lithosphere beneath the Adamawa Uplift (Cameroon, West Africa) Based on gravity data. *Journal of African Earth Sciences* **15**(1), 81–90.

Princivalle, F., Salviulo, G., Fabro, C. & Demarchi, G., 1994. Inter- and intra-crystalline temperature and pressure from NE Brazil mantle xenoliths. *Contributions to Mineralogy and Petrology* **116,** 1–6.

Reisberg, L. & Zindler, A., 1987. Extreme isotopic variations in the upper mantle: evidence from Ronda. *Earth and Planetary Science Letters* **81,** 29–45.

Roden, M. F. & Shimizu, N., 1993. Ion microprobe analyses bearing on the composition of the upper mantle beneath the Basin and Range and Colorado Plateau provinces. *Journal of Geophysical Research* **98**(B8), 14091–14108.

Roden, M. F., Irving, A. J. & Murthy, V. R., 1988. Isotope and trace element composition of the upper mantle beneath a young continental rift: results from Kilbourne Hole, New Mexico. *Geochimica et Cosmochimica Acta* **52,** 461–473.

Schiano, P. & Clocchiatti, R., 1994. Worldwide occurrence of silica-rich melts in sub-continental and sub-oceanic mantle minerals. *Nature* **368,** 621–624.

Shimizu, N. & Richardson, S. H., 1987. Trace element abundance patterns of garnet inclusions in peridotite-suite diamonds. *Geochimica et Cosmochimica Acta* **51,** 755–758

Sibuet, J.-C. & Mascle, J., 1978. Plate kinematic implications of Atlantic equatorial fracture zone trends. *Journal of Geophysical Research* **83,** 3401–3421.

Simkin, T. & Smith, J. V., 1970. Minor element distribution in olivine. *Journal of Geology* **78,** 304–325.

Snyder, G. A., Jerde, E. A., Taylor, L. A., Halliday, A. N., Sobolev, V. N. & Sobolev, N. V., 1993. Nd and Sr isotopes from diamondiferous eclogites, Udachnaya kimberlite pipe, Yakutia, Siberia: evidence of differentiation in the early Earth? *Earth and Planetary Science Letters* **118,** 91–100.

Song, Y. & Frey, F. A., 1989. Geochemistry of peridotite xenoliths in basalt from Hannouba, Eastern China: implications for subcontinental mantle heterogeneity. *Geochimica et Cosmochimica Acta* **53,** 97–113.

Stolz, A. J. & Davies, G. R., 1988. Chemical and isotopic evidence from spinel lherzolite xenoliths for episodic metasomatism of the upper mantle beneath Southeast Australia. *Journal of Petrology, Special Lithosphere Issue,* 303–330.

Stosch, H.-G., 1981. Sc, Cr, Co and Ni partitioning between minerals from spinel peridotite xenoliths. *Contributions to Mineralogy and Petrology* **78,** 166–174.

Stosch, H.-G., 1982. Rare earth element partitioning between minerals from anhydrous spinel peridotite xenoliths. *Geochimica et Cosmochimica Acta* **46,** 793–811.

Stosch, H.-G., Carlson, R. W. & Lugmair, G. W., 1980. Episodic mantle differentiation: Nd and Sr isotopic evidence. *Earth and Planetary Science Letters* **47,** 263–271.

Stosch, H.-G., Lugmair, G. W. & Kovalenko, V. I., 1986. Spinel peridotite xenoliths from the Tariat Depression, Mongolia. II: Geochemistry and Nd and Sr isotopic composition and their implications for the evolution of the subcontinental lithosphere. *Geochimica et Cosmochimica Acta* **50,** 2601–2614.

Stuart, G. W., Fairhead, J. D., Dorbath, L. & Dorbath, C., 1985. A seismic refraction study of the crustal structure associated with the Adamawa Plateau and Garoua Rift, Cameroon, West Africa. *Geophysical Journal of the Royal Astronomical Society* **81,** 1–12.

Stueber, A. M. & Ikramuddin, M., 1974. Rubidium, strontium and barium in ultramafic nodule minerals and host basalts. *Geochimica et Cosmochimica Acta* **38,** 207–216.

Sun, S.-S. & McDonough, W. F., 1989. Chemical and isotopic systematics of oceanic basalts: implications for mantle composition and processes. In: Saunders, A. D. & Norry, M. J. (eds), *Magmatism in the Ocean Basins. Geological Society of London, Special Publication* **42,** 315–345.

Van Houten, F. B., 1983. Sirte Basin, north-central Libya: Cretaceous rifting above a fixed mantle hotspot? *Geology* **11,** 115–118.

Wells, P. R. A., 1977. Pyroxene thermometry in simple and complex systems. *Contributions to Mineralogy and Petrology* **62,** 129–139.

White, W. M. & Hofmann, A. W., 1982. Sr and Nd isotope geochemistry of oceanic basalts and mantle evolution. *Nature* **296,** 821–825.

Wilkinson, J. F. G. & Le Maitre, R. W., 1987. Upper mantle amphiboles and micas and TiO_2, K_2O and P_2O_5 abundances and 100 $Mg/(Mg+Fe^{2+})$ ratios of common basalts and andesites: implications for modal mantle metasomatism and undepleted mantle compositions. *Journal of Petrology* **28,** 37–73.

Witt-Eickschen, G. & Seck, H. A., 1991. Solubility of Ca and Al in orthopyroxene from spinel peridotite: and improved version of an empirical geothermometer. *Contributions to Mineralogy and Petrology* **106,** 431–439.

Zindler, A. & Jagoutz, E., 1988. Mantle cryptology. *Geochimica et Cosmochimica Acta* **52,** 319–333.

Zindler, A., Staudigel, H., Hart, S R., Enders, R. & Goldstein, S., 1983. Nd and Sr isotopic study of a mafic layer from Ronda ultramafic complex. *Nature* **304,** 226–230.

Zipfel, J. & Wörner, G., 1992. Four- and five-phase peridotites from a continental rift system: evidence for upper mantle uplift and cooling at the Ross Sea margin (Antarctica). *Contributions to Mineralogy and Petrology* **111,** 24–36.

RECEIVED JULY 29, 1994

REVISED TYPESCRIPT ACCEPTED OCTOBER 31, 1995